Annals of Pharmacy Practice and Pharmacotherapy
ISSN: 3062-4436
2022, Volume 2, Page No: 155-177

Available online at: www.galaxypub.co/page/journals

Galaxy Publication

PPAR-γ Deubiquitination Mediates the Anti-Senescent Effects of 1, 8-Cineole in Diabetic Vasculature

Andrew J. Collins[1], Sophie R. Turner[2]*, William D. Harris[3]

[1]Department of Pharmacy Practice, School of Pharmacy, University of Otago, Dunedin, New Zealand.
[2]Department of Clinical Pharmacy, Faculty of Pharmacy, University of Sydney, Sydney, Australia.
[3]Department of Pharmacy Practice, Faculty of Pharmacy, University of Toronto, Toronto, Canada.

***E-mail** ✉ s.turner.otago@hotmail.com

Received: 14 January 2021; **Revised:** 10 March 2022; **Accepted:** 11 March 2022

ABSTRACT

Senescence of vascular endothelial cells plays a critical role in the initiation and worsening of cardiovascular complications in diabetes mellitus (DM). Extensive research has established that 1, 8-cineole possesses a broad spectrum of pharmacological activities, such as anti-inflammatory, antimicrobial, and antioxidative effects. This study explored the potential of 1, 8-cineole to improve cardiovascular conditions and endothelial impairment, since its effects and mechanisms in diabetic vascular aging have not been fully clarified. Our data showed clear signs of senescence in both animal and cell-based models. 1, 8-Cineole treatment corrected abnormal lipid levels and diminished vascular aging in diabetic mice. Bioinformatics predictions highlighted peroxisome proliferator-activated receptor-γ (PPAR-γ) as a pivotal player in DM and aging. Direct interaction between 1, 8-cineole and PPAR-γ was confirmed. The effects of 1, 8-cineole were further substantiated using the PPAR-γ activator rosiglitazone, the antagonist GW9662, and PPAR-γ-specific siRNA. In addition, direct binding of 1, 8-cineole to PPAR-γ protein was validated through cellular thermal shift assay, drug affinity responsive target stability testing, and surface plasmon resonance experiments. Overall, these data offer the first proof that 1, 8-cineole counters DM-triggered vascular endothelial aging by enhancing PPAR-γ protein stability via deubiquitination at the Lys-466 position.

Keywords: 1, 8-Cineole, Vascular endothelial cell senescence, Peroxisome proliferator-activated receptor-γ, Ubiquitination

How to Cite This Article: Collins AJ, Turner SR, Harris WD. PPAR-γ Deubiquitination Mediates the Anti-Senescent Effects of 1, 8-Cineole in Diabetic Vasculature. Ann Pharm Pract Pharmacother. 2022;2:155-77. https://doi.org/10.51847/l278zwbQdJ

Introduction

Diabetes mellitus (DM) is a long-term metabolic condition defined by imbalances in glucose, protein, and fat metabolism. Sustained hyperglycemia causes damage and malfunction across numerous organs, with major cardiovascular issues standing out as primary drivers of death [1]. Current investigations have pinpointed vascular aging as a fundamental element in the emergence and advancement of cardiovascular disorders, which remain the top cause of mortality among individuals with type 2 diabetes mellitus (T2DM) [2]. Vascular aging largely stems from the aging of vascular components, most notably endothelial cells [3]. Typical signs of aged vascular endothelial cells encompass morphological changes like flattening and enlargement, positive staining for β-galactosidase, upregulated levels of p53, plasminogen activator inhibitor-1 (PAI-1), cyclin-dependent kinase inhibitor 1A (P21), and cyclin-dependent kinase inhibitor 2A (P16), halted cell cycle progression, secretion of senescence-associated secretory phenotype (SASP) factors, and genomic damage [4, 5]. Multiple signaling proteins have been linked to cardiovascular problems arising from DM. Due to the gravity and multifaceted nature of these issues, discovering fresh drug targets and developing effective therapies are vital. It is also important to identify new agents capable of preventing or treating senescence in diabetic endothelial cells.

Peroxisome proliferator-activated receptor-γ (PPAR-γ) belongs to the nuclear receptor family of ligand-dependent transcription factors and is crucial for managing diverse processes, including insulin responsiveness, fat balance, inflammatory responses, cell growth, and aging [6, 7]. Numerous reports link PPAR-γ to disorders related to aging. Evidence suggests that activating PPAR-γ can lessen aging in vascular smooth muscle cells [8], while controlling the stability of PPAR-γ mRNA might affect cell aging and division [9]. Changes in PPAR-γ activity or durability—especially through post-translational processes like ubiquitination and autophagy—could ease metabolic conditions tied to aging and increase longevity [10-12]. Comprehensive studies on how PPAR-γ is regulated during DM-driven vascular endothelial aging are therefore needed.

The monoterpene compound 1, 8-cineole is mainly extracted from essential oils of plants like eucalyptus and serves as a core component in chemical, food, pharmaceutical, and perfumery sectors. It displays various beneficial actions, including anti-inflammatory, antimicrobial, antioxidative, anticancer, anti-aging, and anti-cell death properties, along with the ability to restore impaired vascular endothelial function [13]. Earlier work from our group indicated that 1, 8-cineole shields human umbilical vein endothelial cells from lipopolysaccharide damage by blocking nuclear factor kappa-B (NF-κB) signaling [14]. It also improves endothelial function in mice through PPAR-γ-mediated suppression of NF-κB [15]. Furthermore, 1, 8-cineole influences diabetic retinopathy via the PPAR-γ/TXNIP axis [16]. Additional findings positioned 1, 8-cineole as a new PPAR-γ activator that lowers gut inflammation [17]. Despite this, the exact ways in which 1, 8-cineole impacts senescence of vascular endothelial cells in DM contexts are not yet defined.

Here, we assessed if 1, 8-cineole could limit senescence in human aortic endothelial cells (HAECs) by engaging the PPAR-γ pathway. On a mechanistic level, 1, 8-cineole was found to bind directly to PPAR-γ and block its degradation via ubiquitination, thus easing diabetic vascular endothelial aging. This represents, to our knowledge, the initial evidence supporting 1, 8-cineole as a valuable option for addressing vascular endothelial cell senescence linked to DM.

Materials and Methods

Reagents

High-purity 1, 8-Cineole (99.0%, catalog no. E111233) was sourced from Aladdin Biochemical Technology (Shanghai, China). Palmitic acid (HY-N0830), rosiglitazone (HY-17386), chloroquine (CQ; HY-17589A), cycloheximide (CHX; HY-12320), MG132 (HY-13259), GW9662 (HY-16578), and pronase E (HY-114158A) were acquired from MedChemExpress (Monmouth Junction, NJ, USA). A reactive oxygen species (ROS) detection kit (S0033S) was obtained from Beyotime Biotechnology (Shanghai, China). A cell cycle analysis kit (KGA9101-50) was purchased from KeyGEN BioTECH (Nanjing, China), and a senescence-associated β-galactosidase (SA-β-gal) staining kit (G1580) from Solarbio Science & Technology (Beijing, China). Kits for measuring triglycerides (TG; A110-1-1), total cholesterol (TC; A111-1-1), low-density lipoprotein cholesterol (LDL; A113-1-1), and high-density lipoprotein cholesterol (HDL; A112-1-1) were supplied by Nanjing Jiancheng Bioengineering Institute (Nanjing, China). Human aortic endothelial cells (HAECs) were provided by Fenghui Biotechnology (Changsha, China). Primary antibodies targeting PPAR-γ (60127-1-Ig), P53 (60283-2-Ig), PAI-1 (66261-1-Ig), P21 (82669-2-RR), P16 (10883-1-AP), ubiquitin (10201-2-AP), HA Tag (51064-2-AP), and Flag Tag (66008-4-Ig) were purchased from Proteintech Group (Wuhan, China). The anti-γ-H2A.X antibody (ab81299) was from Abcam (Danvers, MA, USA), and the anti-GAPDH antibody (MB001) from Bioworld Technology (Nanjing, China). Recombinant PPAR-γ protein (12019-H20B) was obtained from Sino Biological (Beijing, China).

Bioinformatics analysis

Diabetes-related gene expression dataset (GSE250283) was retrieved from the GEO database (https://www.ncbi.nlm.nih.gov/geo/). Differentially expressed genes (DEGs) comparing diabetic and control samples were identified using the "limma" package in R (version 4.3.2), with cutoff criteria of $P < 0.01$ and $|logFC| > 0.2$. To discover genes linked to both diabetes and aging, GSE250283 data were cross-referenced with entries from OMIM (https://omim.org/), GeneCards (https://www.genecards.org/), and DisGeNET (https://disgenet.com/), applying minimum scores of 0.1 (DisGeNET) and 15 (GeneCards). Protein–protein interaction (PPI) networks were built using STRING data (https://cn.string-db.org/) and visualized in Cytoscape version 3.8.0, setting interaction confidence at 0.4 and excluding isolated nodes. Functional enrichment for GO

terms and KEGG pathways among core targets was performed with the "clusterProfiler" R package, with results presented as bubble diagrams.

Molecular docking

Small-molecule structures were downloaded in SDF format from PubChem (https://pubchem.ncbi.nlm.nih.gov/) and converted to PDBQT using Open Babel version 2.3.2. Crystal structures of target proteins—TNF (PDB ID: 2AZ5), PPARGC1A (PDB ID: 6W9L), PPAR-γ (PDB ID: 4A4W), PARP1 (PDB ID: 4ZZZ), NLRP3 (PDB ID: 3QF2), GHRL (PDB ID: 7F9Y), and CST3 (PDB ID: 1G96)—were fetched from the Protein Data Bank. Non-essential water and bound ligands were stripped from proteins in PyMOL 2.3.0. Hydrogens were added and partial charges computed via AutoDockTools, followed by conversion to PDBQT format. Docking simulations between ligands and receptors were run with AutoDock Vina 1.5.7. Binding interactions were examined using the Protein-Ligand Interaction Profiler web tool (https://plip-tool.biotec.tu-dresden.de/plip-web/plip/index), and resulting complexes were rendered visually in PyMOL.

Molecular dynamics (MD) simulation and binding free energy

Simulations were conducted in GROMACS version 2022.3 with the CHARMM36 force field (charmm36-jul2022.ff) for topology generation. Systems were solvated in TIP3P water, and sodium ions were introduced for electroneutrality. Initial equilibration lasted 100 ps each in NVT and NPT ensembles at 300 K. Production runs spanned 100 ns with 2 fs integration steps.

Free energy of binding for the protein–ligand complex was computed using the MMPBSA method via the gmx_MMPBSA tool in GROMACS [18], defined as the difference between solvation energy and vacuum potential energy. This approach quantified the interaction strength of 1, 8-cineole with PPAR-γ and highlighted key residue contributions to stability.

Cellular thermal shift assay (CETSA)

HAECs were grown overnight in 10 cm culture dishes. Following 2-hour incubation with either 1, 8-cineole (50 nM) or vehicle (DMSO), cells were rinsed thrice in PBS. Suspensions were distributed into 0.2 mL PCR tubes and exposed to graded temperatures for 3 minutes. Two cycles of freeze-thawing in liquid nitrogen were applied, after which samples were spun at 12, 000 rpm for 15 minutes. Clear supernatants were harvested and analyzed by Western blot to determine changes in protein thermostability.

Drug affinity responsive target stability (DARTS)

Human aortic endothelial cells (HAECs) underwent 3-hour exposure to elevated palmitic acid and glucose (PA/HG). Proteins were harvested in lysis buffer supplemented with 1% PMSF (Solarbio), and concentrations were quantified via BCA kit (Solarbio). Each reaction was normalized to 500 μg total protein. Lysates were then incubated with either 1, 8-cineole (10 or 50 nM) or DMSO control for 1 hour at ambient temperature. Digestion was initiated by adding pronase E (10 mg/mL) at a 1:200 (protein:enzyme) ratio, followed by 10 minutes of proteolysis at room temperature. Reactions were terminated, and resistance to digestion for candidate targets was detected through Western blot analysis.

Surface plasmon resonance (SPR)

Direct binding parameters between 1, 8-cineole and PPAR-γ were determined on a Biacore T200 platform (Cytiva, Wilmington, DE, USA). The CM5 chip surface was activated for 420 seconds using a 400 mM EDC/100 mM NHS mixture delivered at 10 μL/min. Recombinant PPAR-γ (40 μg/mL in coupling buffer) was immobilized onto the active flow cell (Fc2) at 10 μL/min. Residual reactive sites were blocked with 1 M ethanolamine-HCl for 420 seconds at 10 μL/min. Gradient concentrations of 1, 8-cineole (100, 50, 25, 12.5, 6.25, 3.125, and 0 μM) in running buffer were injected across both reference (Fc1) and active (Fc2) cells at 30 μL/min, allowing 120 seconds for association and 200 seconds for dissociation. All kinetic runs were performed with buffer controls, and data from the seven concentrations were evaluated in order of increasing analyte strength.

Animals

Male C57BL/6J mice aged 8 weeks (from Guizhou Medical University Animal Center, License SYXK[Qian] 2018-0001) were kept in pathogen-free housing and split randomly into normal chow or high-fat diet (HFD) cohorts at room temperature.

Following 12 weeks on respective diets, fasting tail blood was taken for HOMA-IR calculation based on glucose and insulin measurements. An IPGTT was conducted by injecting 20% glucose (2 g/kg i.p.), with glucose readings taken at 0, 15, 30, 60, 90, 120, and 150 minutes via glucometer.

After a 1-week adaptation period, diabetes induction involved four consecutive daily i.p. doses of STZ (30 mg/kg in 0.1 M citrate buffer). Animals displaying classic signs (polydipsia, polyuria) and FBG exceeding 11.1 mM were confirmed as diabetic and reassigned into four subgroups: (1) untreated diabetic model; (2) 1, 8-cineole low dose (100 mg/kg, 1, 8-cineole-L); (3) 1, 8-cineole high dose (200 mg/kg, 1, 8-cineole-H); (4) metformin positive control (250 mg/kg, Met). Non-diabetic controls received standard diet plus volume-matched 0.9% NaCl injections; the model group received NaCl only. Interventions continued for 8 weeks before terminal collection under isoflurane anesthesia. Blood serum and tissues, including thoracic aortas (fixed in 4% paraformaldehyde or liquid nitrogen snap-frozen), were harvested. Experiments complied with NIH guidelines and received approval from Guizhou Medical University Ethics Committee (No. 2200045).

For PPAR-γ loss-of-function studies, diabetic mice on HFD received tail-vein delivery of either AD-shPPAR-γ or control AD-NC vectors. After six weeks with or without concurrent 1, 8-cineole, animals were categorized into six arms: control + AD-NC, model + AD-NC, model + 200 mg/kg 1, 8-cineole + AD-NC, control + AD-shPPAR-γ, model + AD-shPPAR-γ, and model + 200 mg/kg 1, 8-cineole + AD-shPPAR-γ. Adenoviral constructs were produced by GenePharma (Shanghai, China); shPPAR-γ target sequence: 5′-AAGCTCCAAGAATACCAAAGT-3′; scrambled NC sequence: 5′-TTCTCCGAACGTGTCACGT-3′. Transgene expression in arteries was confirmed by Nikon fluorescence microscopy two weeks after administration.

Cell culture and treatment

HAECs were propagated in complete endothelial cell medium (ECM) containing 1% penicillin–streptomycin, 5% FBS, and 1% growth supplement at 37 °C under 5% CO_2. Prior to challenge, cells received 1-hour pretreatment with 1, 8-cineole, metformin, GW9662, or rosiglitazone, followed by 48-hour exposure to PA/HG mixture.

Serum biochemical assays

Circulating TG, TC, LDL, and HDL concentrations were determined enzymatically using manufacturer-supplied diagnostic kits.

Histological analysis

Isolated thoracic aortas fixed in 4% paraformaldehyde were paraffin-embedded and sectioned. Vascular morphology was evaluated by HE staining, and fibrosis/collagen content by Masson trichrome. Photomicrographs and measurements were recorded on a Nikon microscope system (Tokyo, Japan).

Immunofluorescence assay

Adapted immunofluorescence protocols were applied. Cultured cells were PBS-rinsed, fixed (4% paraformaldehyde, 30 min, room temperature), and permeabilized (0.2% Triton X-100, 15 min). Non-specific binding was blocked with 5% goat serum (2 h, room temperature). Anti-γ-H2A.X primary antibody was incubated overnight at 4 °C. Following three PBS washes, compatible fluorescent secondary antibody was added for 2 hours at room temperature. Two additional PBS rinses preceded 3-minute dark DAPI nuclear counterstaining. Images were captured on a fluorescence microscope.

Aortic cryosections or paraffin sections underwent analogous staining for PPAR-γ, P53, PAI-1, P21, P16, and γ-H2A.X localization. Fluorescent signals were viewed microscopically and semi-quantified with ImageJ software (version 1.52a).

Enzyme-linked immunosorbent assay (ELISA)

Concentrations of HMGB1, TNF-α, IL-6, and IL-8 in both serum and culture media were determined with specific commercial ELISA kits (Fan Yin, Shanghai, China), strictly adhering to the supplier's guidelines.

ROS assays

Cells underwent three washes in serum-free ECM before being loaded with 10 μM DCFH-DA probe and incubated for 20 min at 37 °C. Post-incubation, another triple wash in serum-free ECM was performed. Fluorescence intensity reflecting ROS production was quantified via flow cytometry on an ACEA NovoCyte system (Hangzhou, China).

SA-β-gal staining

Following PBS rinsing, cells were fixed in the provided solution for 15–20 min. Fixative was removed, cells washed in PBS, and then overlaid with freshly prepared staining mixture (X-Gal : solution A : solution B : solution C = 5:1:1:93 by volume) for overnight incubation at 37 °C. Senescence-associated β-galactosidase activity was visualized and photographed under a Nikon bright-field microscope at 200×. Blue-stained positive cells were enumerated across fields, and the proportion of senescent cells was expressed as a percentage of the total cell count.

Cell cycle assays

Detached cells were PBS-washed and fixed in 70% cold ethanol overnight at 4 °C. After fixation, cells were incubated in the dark for 30–60 min at room temperature with propidium iodide/RNase A staining solution (9:1). DNA content and cycle phase proportions were assessed by flow cytometry, with results analyzed in NovoExpressTM software.

Western blotting analysis

Protein lysates from cultured cells and aortic specimens were obtained in buffer containing 1% PMSF. Following 20-min centrifugation at 12, 000 rpm (4 °C), concentrations were quantified by BCA method. Samples were electrophoresed on 10% or 12% SDS-PAGE gels, electroblotted onto PVDF membranes, and blocked for 2 h in 5% BSA. Overnight incubation at 4 °C with primary antibodies—PPAR-γ (1:1, 000), P53 (1:5, 000), PAI-1 (1:5, 000), P21 (1:2, 000), P16 (1:5, 000), Flag (1:4, 000), HA (1:4, 000), GAPDH (1:10, 000)—was followed by 2-h room-temperature secondary antibody exposure and three TBST rinses. Signals were developed with ECL substrate and captured using a Bio-Rad ChemiDoc XRS+ imager (Bio-Rad Laboratories, Hercules, CA, USA).

Reverse transcription quantitative real-time PCR (RT-qPCR)

Cellular total RNA was purified with TransZol Up (TransGen Biotech, Beijing, China). cDNA synthesis employed the EasyScript® One-Step gDNA Removal and cDNA Synthesis SuperMix (TransGen Biotech). Amplification reactions utilized PerfectStart® Green qPCR SuperMix (TransGen Biotech) on a Bio-Rad CFX Manager 3.1 instrument (Bio-Rad Laboratories). Fold changes in mRNA were computed via the $2^{-\Delta\Delta Ct}$ approach, with GAPDH serving as internal control. All primer pairs are detailed in **Table 1**.

Table 1. Quantitative reverse-transcription polymerase chain reaction primers.

Gene Alias	Forward Primer (5′-3′)	Reverse Primer (5′-3′)
Peroxisome proliferator-activated receptor-γ	PPAR-γ	CCAGAAGCCTGCATTTCTGC
Tumor protein p53	P53	AAAGTCTAGAGCCACCGTCC
Plasminogen activator inhibitor-1	PAI-1	TGAACGAGAGTGGCACGGT
Cyclin-dependent kinase inhibitor 1A	P21	GCCGAAGTCAGTTCCTTGTG
Cyclin-dependent kinase inhibitor 2A	P16	GCCACAAAAGCCATTCACGA
Glyceraldehyde 3-phosphate dehydrogenase	GAPDH	CATGGCCGTGTAGGAGACTCA

siRNA transfection

Transient knockdown in HAECs was achieved by delivering human PPAR-γ-specific or scrambled control siRNA oligomers using Lipofectamine 2000 as per protocol. PPAR-γ siRNA duplex sequences: sense 5′-GACACAGAGAUGCCAUUCUTT-3′, antisense 5′-AGAAUGGCAUCUCUGUGUCTT-3′. Control sequences: sense 5′-UUCUCCGAACGUGUCACGUTT-3′, antisense 5′-ACGUGACACGUUCGGAGAATT-3′. Successful silencing was confirmed through Western blot and RT-qPCR.

Plasmid transfection

GenePharma supplied Flag-PPAR-γ constructs (wild-type and mutants K170R, K466R, K485R) along with HA-Ub and vector controls; mutants featured lysine-to-arginine substitutions at indicated sites. HEK293T cells received Lipofectamine 2000-mediated transfection per instructions. Eight hours after introducing designated Flag-PPAR-γ and HA-Ub plasmids, cultures were treated for 48 h with 50 nM 1, 8-cineole combined with 10 μM MG132 prior to collection for subsequent immunoprecipitation assays.

IP assays

Protein was isolated and measured in immunoprecipitation buffer containing both phosphatase and protease inhibitors. Whole lysates were rotated overnight with antibodies against PPAR-γ, IgG (control), or Flag. Pull-down was executed with a ready-to-use immunoprecipitation kit from Sangon Biotechnology (Shanghai, China). Enriched PPAR-γ, ubiquitin, Flag-tagged, and HA-tagged proteins were then examined via Western blot.

Mass spectrometry analysis

Following lysis, PPAR-γ ubiquitination sites were mapped by overnight pull-down at 4 °C using anti-PPAR-γ antibody. Captured protein was run on SDS-PAGE, and target bands were cut out for digestion. Peptides were sequenced and analyzed by LC-MS/MS to pinpoint modification sites.

Statistical analysis

All analyses were conducted in GraphPad Prism version 8. Values are reported as mean ± SD based on a minimum of three separate experiments. Multiple comparisons used one-way ANOVA with Tukey's post-test, while direct pairwise comparisons employed unpaired two-tailed Student's t-test. Results were deemed significant when $P < 0.05$.

Results and Discussion

PPAR-γ emerges as a candidate target in diabetes-associated aging

Comparison of diabetic versus non-diabetic samples yielded 2, 952 differentially expressed genes. Cross-referencing databases (OMIM, GeneCards, DisGeNET) produced 901 diabetes-linked targets and 717 aging-linked targets. Overlap analysis via Venn diagram identified eight shared candidates worthy of further scrutiny for dual therapeutic potential **(Figure 1a)**. These comprised PPARGC1A, TNF, GHRL, PPAR-γ, PARP1, DDOST, NLRP3, and CST3. A protein interaction network was generated, followed by enrichment studies. Removal of isolated nodes left seven interconnected hubs, dropping DDOST **(Figure 1b)**. Leading biological process terms encompassed circadian rhythm, rhythmic processes, and downregulation of external stimulus responses. Cellular component analysis ranked endoplasmic reticulum lumen, oligosaccharyltransferase complex, and canonical inflammasome complex highest **(Figure 1c)**. Given the established role of chronic inflammation in aging, PPAR-γ linkage to the inflammasome complex hinted at its contribution to inflammatory aging pathways. Top molecular functions involved DNA-binding transcription factor activity, nuclear receptor activity, and RNA polymerase II-specific transcription regulation. KEGG pathways prominently featured necroptosis, lipid and atherosclerosis, longevity regulation, and insulin resistance **(Figure 1d)**. PPAR-γ specifically mapped to lipid/atherosclerosis, longevity, AMPK signaling, osteoclast differentiation, and non-alcoholic fatty liver disease routes, highlighting its dual involvement in metabolic control and lifespan modulation. Docking simulations tested 1, 8-cineole affinity against all eight proteins. Energies < −5 kcal/mol signaled robust binding. Favorable scores were obtained for PPARGC1A, TNF, GHRL, PPAR-γ, PARP1, DDOST, and NLRP3, supporting possible intervention in diabetes-driven aging through these interactions **(Figures 1e–1l)**. TNF docking scored −5.9 kcal/mol. In light of GO ties between PPAR-γ and inflammasome components, potential modulation of inflammatory markers like TNF-α by 1, 8-cineole was noted. Key contacts occurred at ARG-288, LYS-265, and PHE-287 of PPAR-γ, yielding −5.7 kcal/mol and marking PPAR-γ as the standout candidate for 1, 8-cineole action in diabetes-related aging. Supporting KEGG data placed PPAR-γ centrally in lipid, atherosclerotic, and longevity networks. Together with earlier findings [19], this reinforces PPAR-γ centrality in diabetes-linked lipid disturbance and aging, warranting deeper mechanistic exploration, which we pursued next.

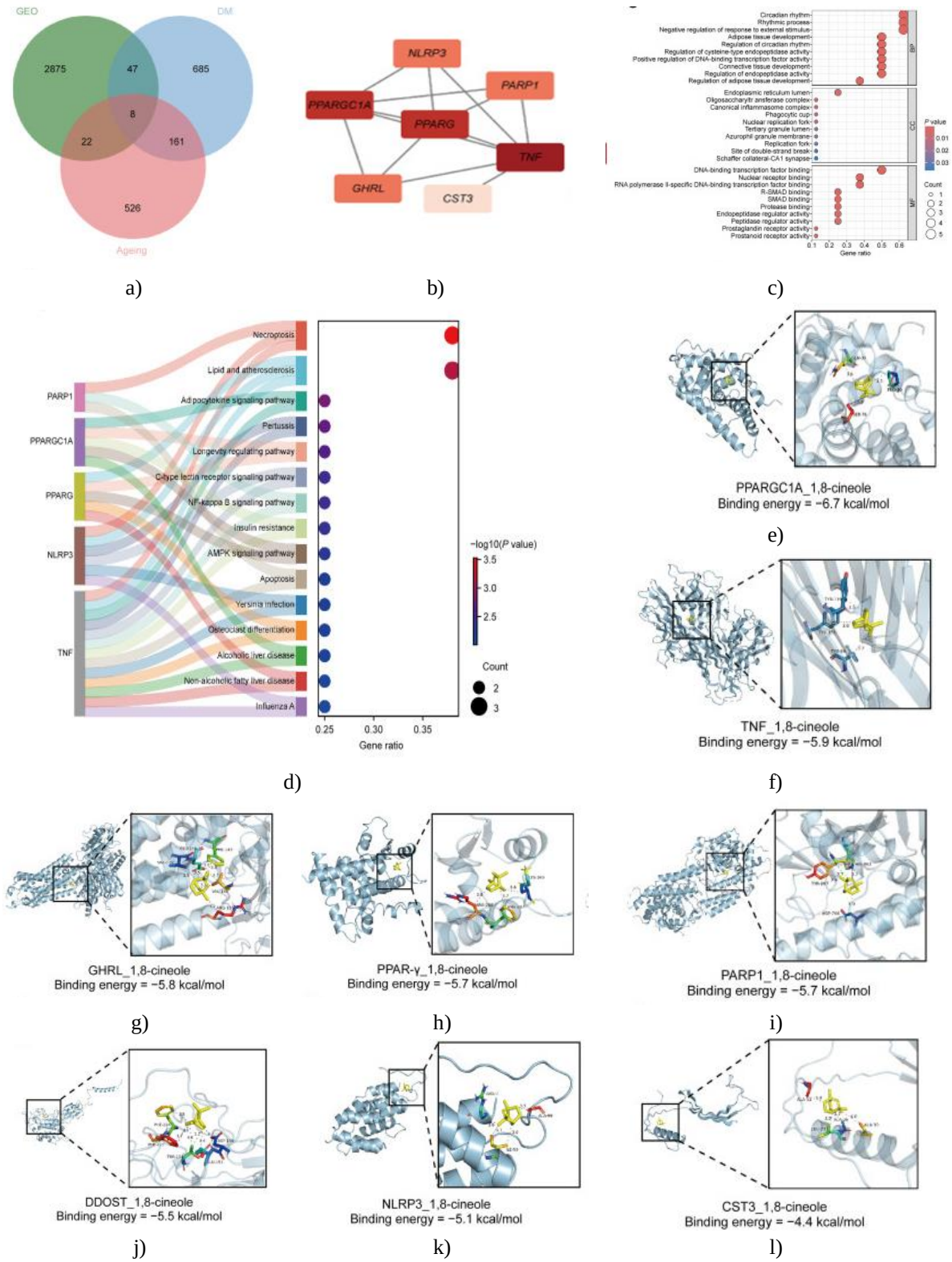

a) b) c) d) e) f) g) h) i) j) k) l)

Figure 1. Bioinformatics screening for candidate aging targets in diabetes mellitus (DM). (a) Venn diagram displaying target overlap across four sources. (b) Protein–protein interaction (PPI) network among core genes. (c, d) Gene Ontology (GO) enrichment (c) and Kyoto Encyclopedia of Genes and Genomes (KEGG) pathway analysis (d) for candidate targets. (e–l) Docking poses of 1, 8-cineole with peroxisome proliferator-activated receptor gamma coactivator 1 alpha (PPARGC1A) (E), tumor necrosis factor (TNF) (f), ghrelin (GHRL) (g), peroxisome proliferator-activated receptor-γ (PPAR-γ) (h), poly (ADP-ribose) polymerase (PARP1) (i), dolichyl diphosphooligo-saccharide-protein glycosyltransferase (DDOST) (j), NLR family, pyrin domain containing protein 3 (NLRP3) (k) and cystatin 3 (CST3) (l).

MD simulation validation

Through molecular dynamics trajectories, we tracked real-time binding behaviour, individual residue movements, domain shifts, and overall complex integrity. RMSD serves as a key indicator of structural equilibrium by measuring average atomic displacement over time. In the 1, 8-cineole–PPAR-γ system, RMSD showed initial sharp variations and a rapid drop in the opening nanoseconds—typical when starting from a rigid docking pose that requires relaxation. As interactions refined, the system settled, with RMSD converging after approximately 60 ns to a plateau around 0.64 nm, demonstrating sustained binding consistency **(Figure 2a)**. Radius of gyration (Rg) assesses compactness; stable Rg readings confirmed that ligand engagement did not disrupt the protein's global fold **(Figure 2b)**. Per-residue flexibility, captured by RMSF, was notably higher in the PPAR-γ region spanning residues 416–443 compared to the rest of the structure **(Figure 2c)**. Buried solvent-accessible surface area (SASA) reflects interface stability; constant buried SASA values indicated persistent contact between ligand and protein **(Figure 2d)**. Binding free energy, computed with gmx_MMPBSA, totalled −17.81 kcal/mol **(Table 2)**. Decomposition per residue revealed specific amino acids driving favourable or unfavourable contributions to complex formation **(Figure 2e)**. These collective parameters underscore strong, energetically favourable, and dynamically stable interaction of 1, 8-cineole with PPAR-γ.

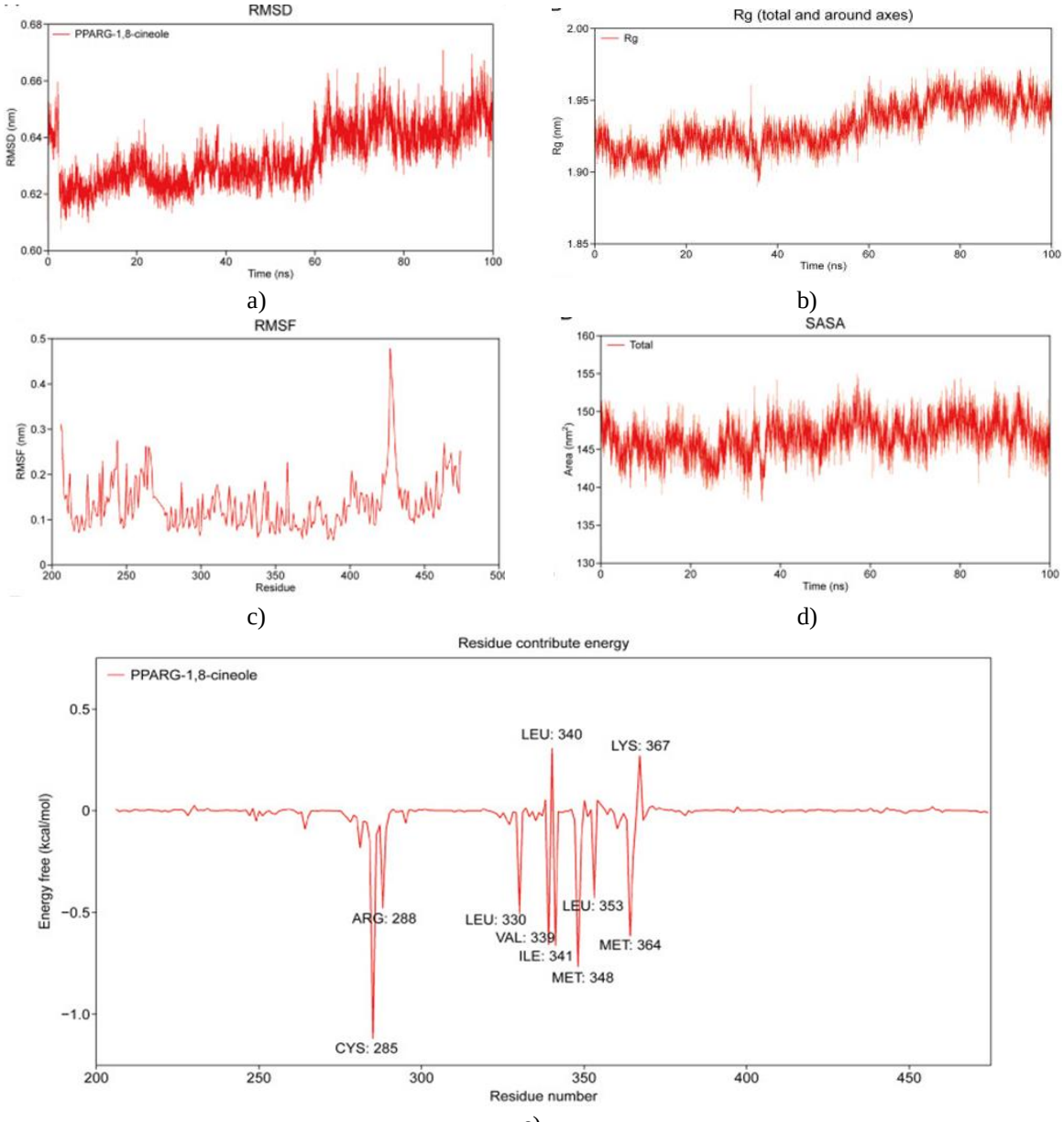

Figure 2. Molecular dynamics (MD) simulation of 1, 8-cineole–peroxisome proliferator-activated receptor-γ (PPAR-γ) binding and decomposition analysis of binding free energy and residue capacity. (a) Root-mean-

square-deviation (RMSD), (b) radius of gyration (Rg), (c) root mean square fluctuation (RMSF), and (d) solvent accessible surface area (SASA) values. (e) Energy breakdown of amino acid residues. CYS: cysteine; ARG: arginine; LEU: leucine; VAL: valine; ILE: isoleucine; MET: methionine; LYS: lysine.

Table 2. Energy decomposition of the complex of 1, 8-cineole with peroxisome proliferator-activated receptor-γ (PPAR-γ) protein in molecular dynamics (MD) simulation.

Energy Component	Average (kcal/mol)	SD
VDWAALS	−20.31	1.34
EEL	−0.41	0.61
EPB	5.42	1.01
ENPOLAR	−2.5	0.07
GGAS	−20.72	1.49
GSOLV	2.92	0.97
Total	−17.81	1.45

EEL: electrostatic energy; EPB: electrostatic polar solvation energy; ENPOLAR: non-polar solvation energy; GGAS: gas-phase free energy; GSOLV: solvation free energy; VDWAALS: van der waals energy; SD: standard deviation.

PPAR-γ is a promising potential therapeutic target of 1, 8-cineole

CETSA has proven valuable for confirming drug–target interactions in cellular contexts. Exposure to 1, 8-cineole substantially raised the melting temperature of PPAR-γ **(Figures 3a and 3b)**. Complementary DARTS data revealed enhanced resistance of PPAR-γ to enzymatic digestion in the presence of 1, 8-cineole **(Figures 3c and 3d)**. SPR kinetics directly measured association, establishing a binding affinity of 23.8 μM between 1, 8-cineole and PPAR-γ **(Figure 3e)**. Converging evidence from these independent techniques verifies direct engagement and consequent stabilisation of PPAR-γ by 1, 8-cineole, solidifying its status as the compound's principal target.

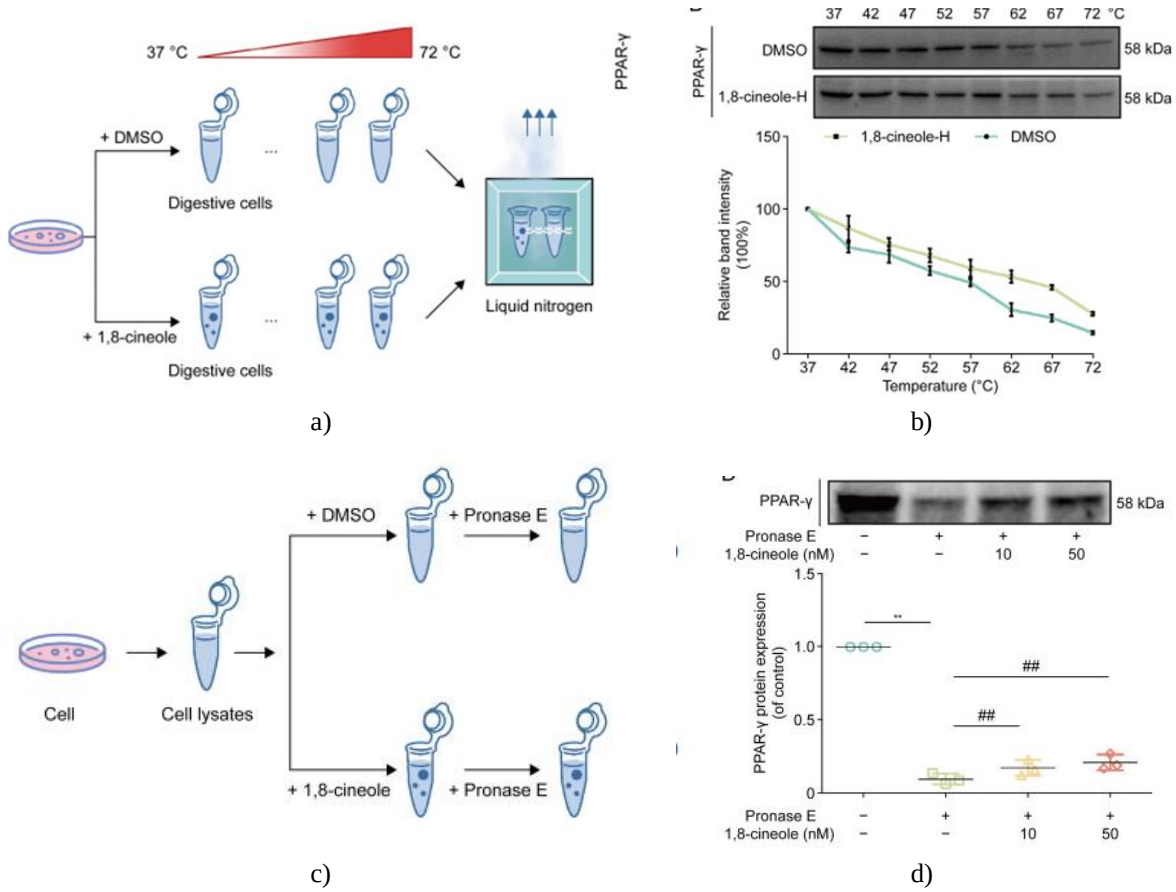

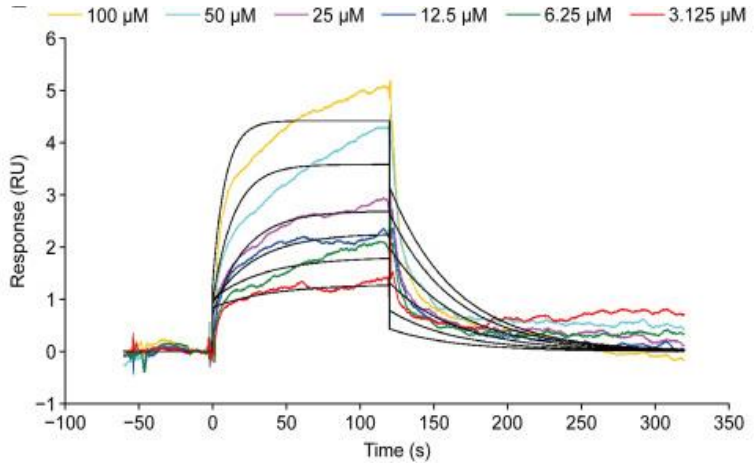

e)

Figure 3. Peroxisome proliferator-activated receptor-γ (PPAR-γ) is a key target of 1, 8-cineole. (a) Cellular thermal shift assay (CETSA) flowchart. (b) Western blotting results of the CETSA experiment indicating improved PPAR-γ heat stability after 1, 8-cineole treatment (n = 3). (c) Drug affinity responsive target stability (DARTS) assay flowchart. (d) Western blotting results of the DARTS experiment indicating that the PPAR-γ protein was more tolerant to pronase E after 1, 8-cineole treatment (n = 3). (e) Surface plasmon resonance (SPR) analysis results of 1, 8-cineole and PPAR-γ showing an affinity constant of 23.8 μM. Data are represented as mean ± standard deviation (SD). ∗∗P < 0.01 vs. the control, ##P < 0.01 vs. pronase E; NS: no significance. DMSO: dimethyl sulfoxide; 1, 8-cineole-H: high-dose 1, 8-cineole.

1, 8-Cineole ameliorates lipid metabolism and vascular histopathological injury in HFD/STZ-induced T2DM mice

The combined high-fat diet and streptozotocin regimen reliably recapitulates core type 2 diabetes features such as sustained hyperglycemia, defective glucose handling, and insulin resistance [20]. The in vivo study scheme is depicted in **Figure 4a**. Following 12 weeks of HFD plus STZ challenge, diabetic animals exhibited clear deficits in glucose clearance, heightened insulin resistance indices, and elevated blood glucose relative to controls, verifying effective disease induction **(Figures 4b–4e)**. Longitudinal fasting glucose tracking during intervention showed robust reduction by metformin, whereas 1, 8-cineole exerted no notable glucose-lowering versus untreated diabetics. Aortic pathology via HE staining in models revealed hallmark diabetic alterations: wall thickening and protrusion, matrix disarray, and fibre wandering; Masson staining exposed excessive collagen buildup and disrupted elastic networks. Both 1, 8-cineole and metformin markedly corrected these structural defects **(Figure 4f)**. Serum lipid assessment disclosed typical dyslipidemia in models—reduced HDL alongside heightened TG, TC, and LDL—which 1, 8-cineole significantly counteracted across all metrics **(Figures 4g–4j)**. Circulating pro-inflammatory mediators HMGB1, TNF-α, IL-6, and IL-8 rose sharply in diabetic mice but were dampened by 1, 8-cineole, pointing to suppression of aging-linked inflammatory signatures **(Figures 4k–4n)**. In aggregate, 1, 8-cineole demonstrates clear potential to rectify lipid imbalances and reverse vascular structural damage in this T2DM model.

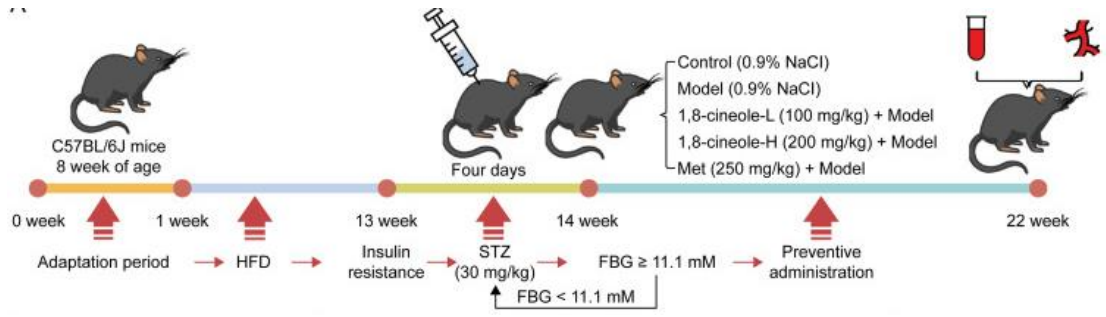

a)

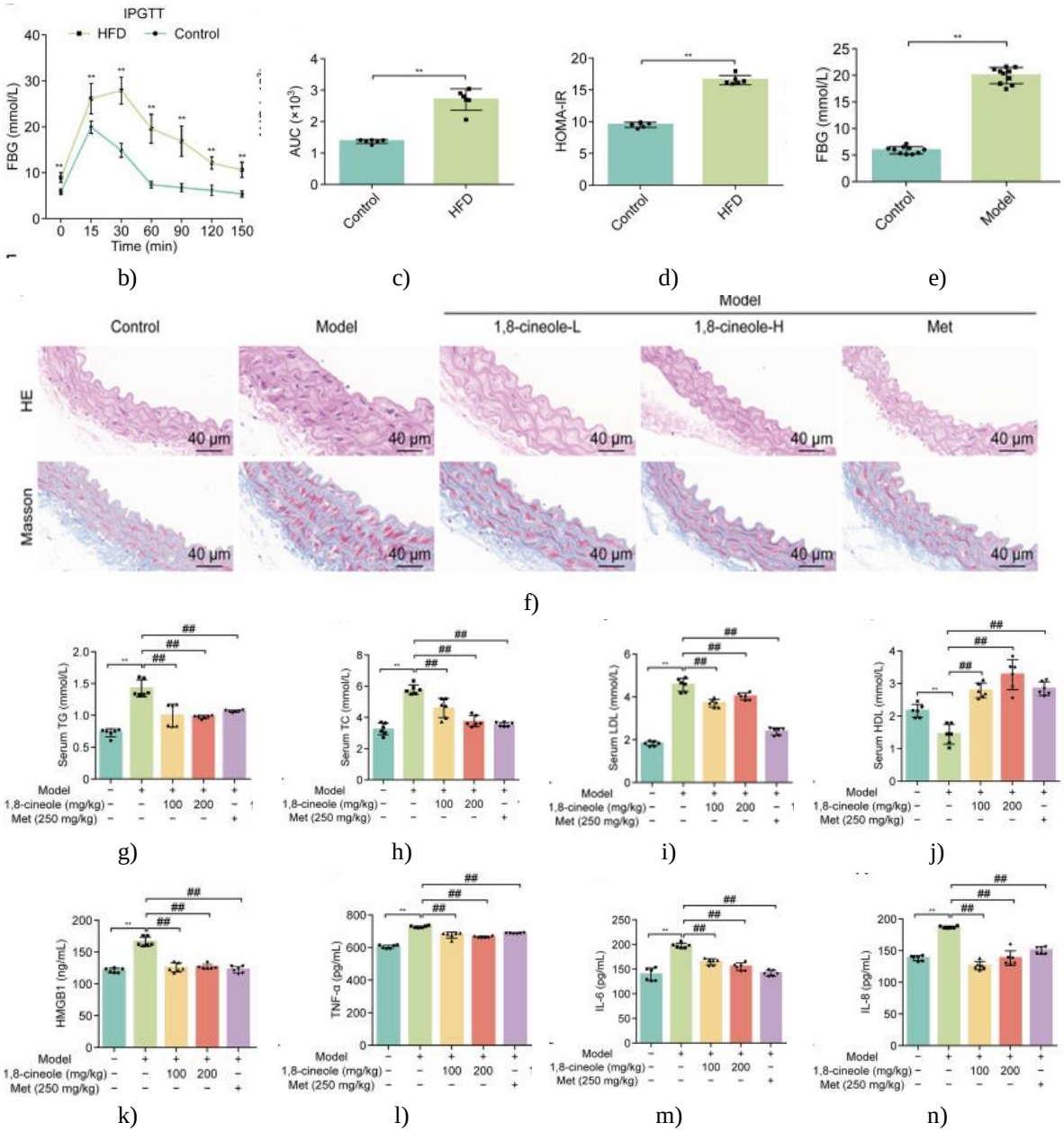

Figure 4. 1, 8-Cineole corrects disrupted lipid handling and aortic structural damage in type 2 diabetes mellitus (T2DM) mice. (a) Outline of the protocol for inducing T2DM in mice and delivering 1, 8-cineole. (b) Serial blood glucose readings taken during fasting after intraperitoneal delivery of 20% glucose (n = 6). (c) Area under the curve (AUC) derived from intraperitoneal glucose tolerance test (IPGTT) data. (d) Homeostasis model assessment of insulin resistance (HOMA-IR) scores across groups (n = 6). (e) Fasting blood glucose (FBG) readings once the T2DM model was confirmed (n = 10). (f) Typical haematoxylin and eosin (HE) along with Masson trichrome images of aortic samples (n = 3). (G–J) Circulating levels of triglycerides (TG) (g), total cholesterol (TC) (h), low-density lipoprotein cholesterol (LDL) (i), and high-density lipoprotein cholesterol (HDL) (j) across cohorts (n = 6). (k–n) Circulating concentrations of high mobility group box 1 (HMGB1) (k), tumor necrosis factor-α (TNF-α) (l), interleukin-6 (IL-6) (m), and interleukin-8 (IL-8) (n) in the animals (n = 6). Values are expressed as mean ± standard deviation (SD). ∗∗P < 0.01 vs. the control, ##P < 0.01 vs. the model. Met: metformin; 1, 8-cineole-L: low-dose 1, 8-cineole; 1, 8-cineole-H: high-dose 1, 8-cineole; HFD: high-fat diet; STZ: streptozotocin; AUC: Area under the curve.

1, 8-Cineole reduces thoracic aortic vascular aging in T2DM mice

Existing literature identifies vascular aging as a major driver of cardiovascular issues in T2DM [21]. To probe whether 1, 8-cineole offers protection against this process, we examined senescence-associated markers via

immunofluorescence and Western blotting. Model mice exhibited substantial elevations in P53, PAI-1, P21, and P16 alongside a drop in PPAR-γ compared to controls **(Figures 5a–5f)**. Administration of 1, 8-cineole effectively restored more normal expression patterns. The DNA damage marker γ-H2A.X, known to promote vascular impairment and aging in diabetes [22, 23], was visualised in aortic tissue by immunofluorescence. Its abundance rose sharply in models but fell markedly with 1, 8-cineole intervention **(Figures 5g and 5h)**. These immunofluorescence observations were corroborated by Western blot quantification of the same proteins in aortic homogenates **(Figures 5i and 5j)**. In summary, 1, 8-cineole actively suppresses diabetes-associated vascular aging.

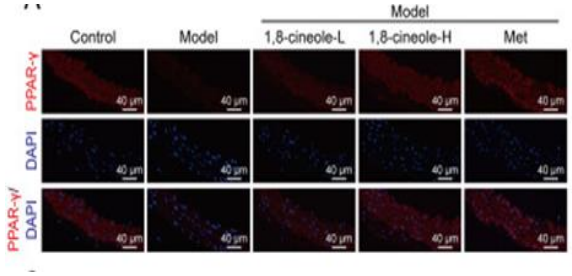

a)

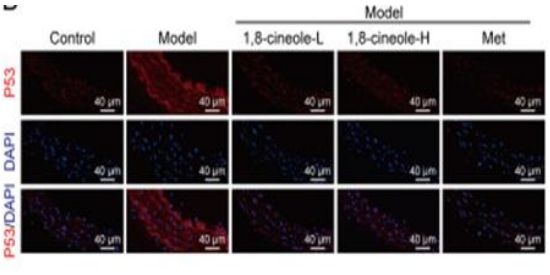

b)

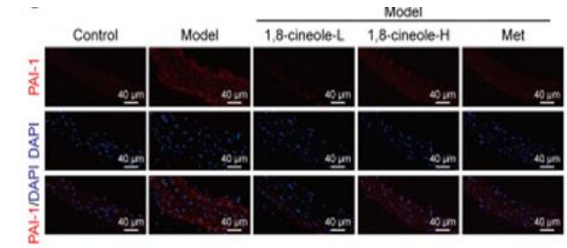

c)

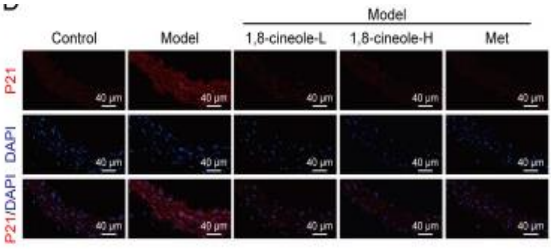

d)

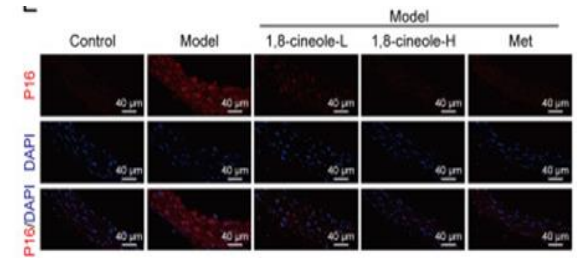

e)

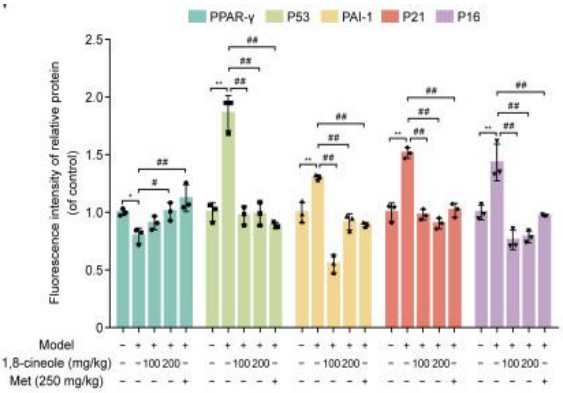

f)

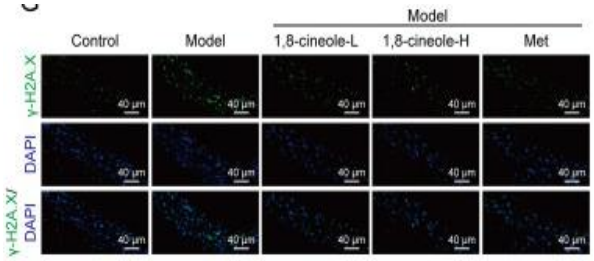

g)

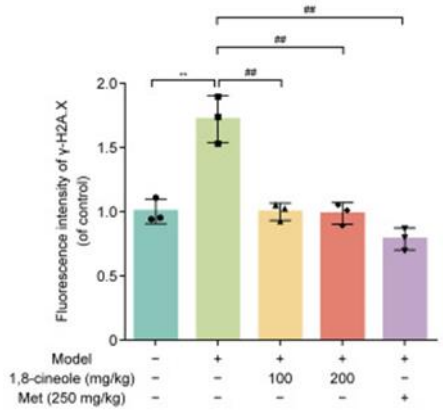

h)

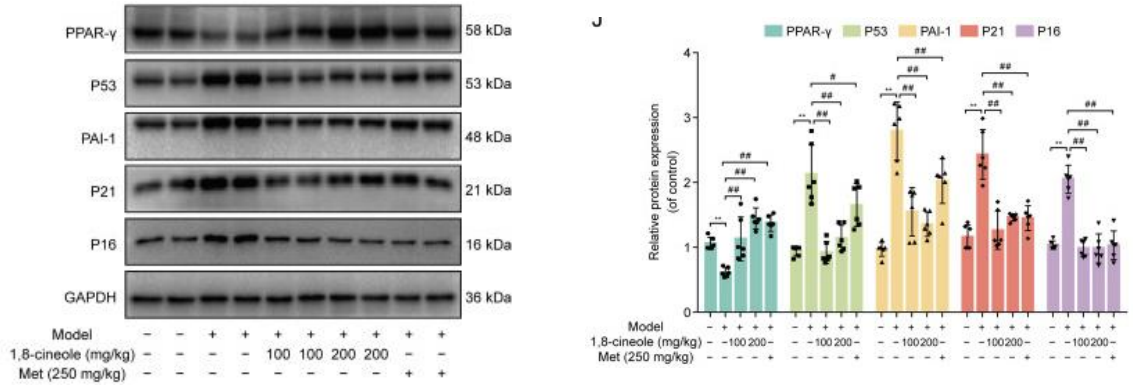

i) j)

Figure 5. 1, 8-Cineole curbs vascular aging in type 2 diabetes mellitus (T2DM) mice. (a–e) Immunofluorescent detection of peroxisome proliferator-activated receptor-γ (PPAR-γ) (a), p53 (b), plasminogen activator inhibitor-1 (PAI-1) (c), cyclin-dependent kinase inhibitor 1A (P21) (d), and cyclin-dependent kinase inhibitor 2A (P16) (e) within thoracic aortic walls. (f) Quantified immunofluorescence signals for PPAR-γ, P53, PAI-1, P21, and P16 (n = 3). (g) Immunofluorescent visualisation of γ-H2A.X in aortic sections. (h) Quantified γ-H2A.X fluorescence intensity (n = 3). (i) Western blot profiling of PPAR-γ, P53, PAI-1, P21, and P16 from aortic extracts. (j) Densitometry-based quantification of the Western blots for PPAR-γ, P53, PAI-1, P21, and P16 (n = 6). Values are mean ± standard deviation (SD). ∗P < 0.05 and ∗∗P < 0.01 vs. the control, #P < 0.05 and ##P < 0.01 vs. the model. 1, 8-cineole-L: low-dose 1, 8-cineole; 1, 8-cineole-H: high-dose 1, 8-cineole; DAPI: 4′, 6-diamidino-2-phenylindole; Met: metformin; GAPDH: glyceraldehyde 3-phosphate dehydrogenase.

1, 8-Cineole counters PA/HG-triggered senescence in HAECs

Viability screening via CCK-8 assay guided selection of 10 and 50 nM 1, 8-cineole as safe working concentrations for downstream experiments. To gauge anti-senescence efficacy, SA-β-gal activity was monitored in PA/HG-stressed HAECs. Exposure to PA/HG drove a sharp rise in positively stained cells, which 1, 8-cineole pretreatment robustly diminished **(Figures 6a and 6b)**. Flow cytometry further showed that 1, 8-cineole prevented the pronounced G0/G1 blockade induced by PA/HG **(Figures 6c and 6d)**. Protein analysis of senescence indicators revealed PA/HG-mediated increases in P53, PAI-1, P21, and P16 coupled with PPAR-γ suppression; prior exposure to 1, 8-cineole reversed this profile, boosting PPAR-γ while curbing the senescence markers **(Figures 6e and 6f)**. Collectively, these findings establish that 1, 8-cineole shields HAECs against PA/HG-evoked senescence, likely through engagement with PPAR-γ.

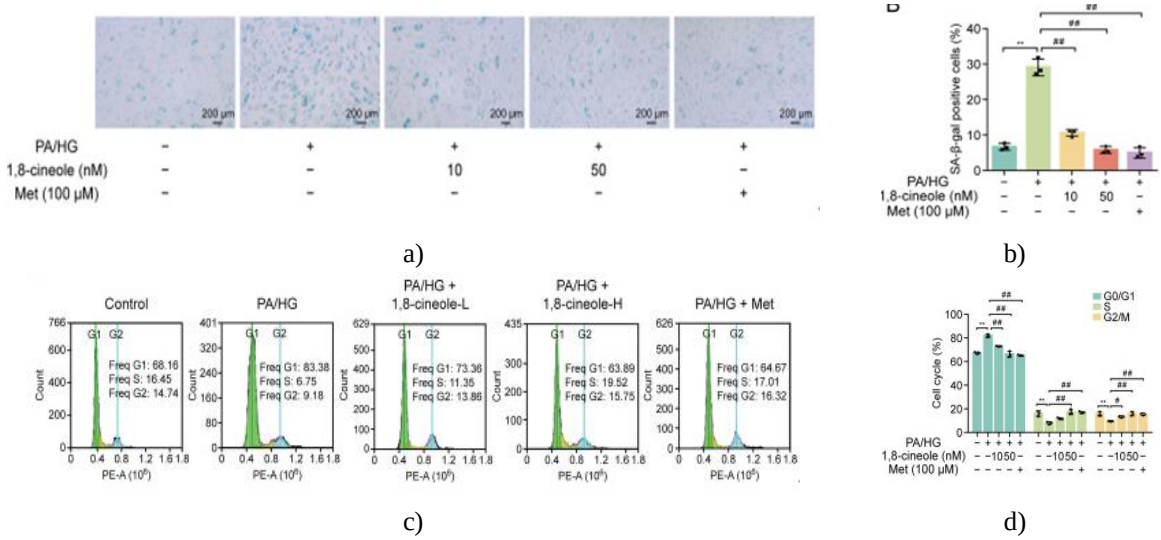

a) b)

c) d)

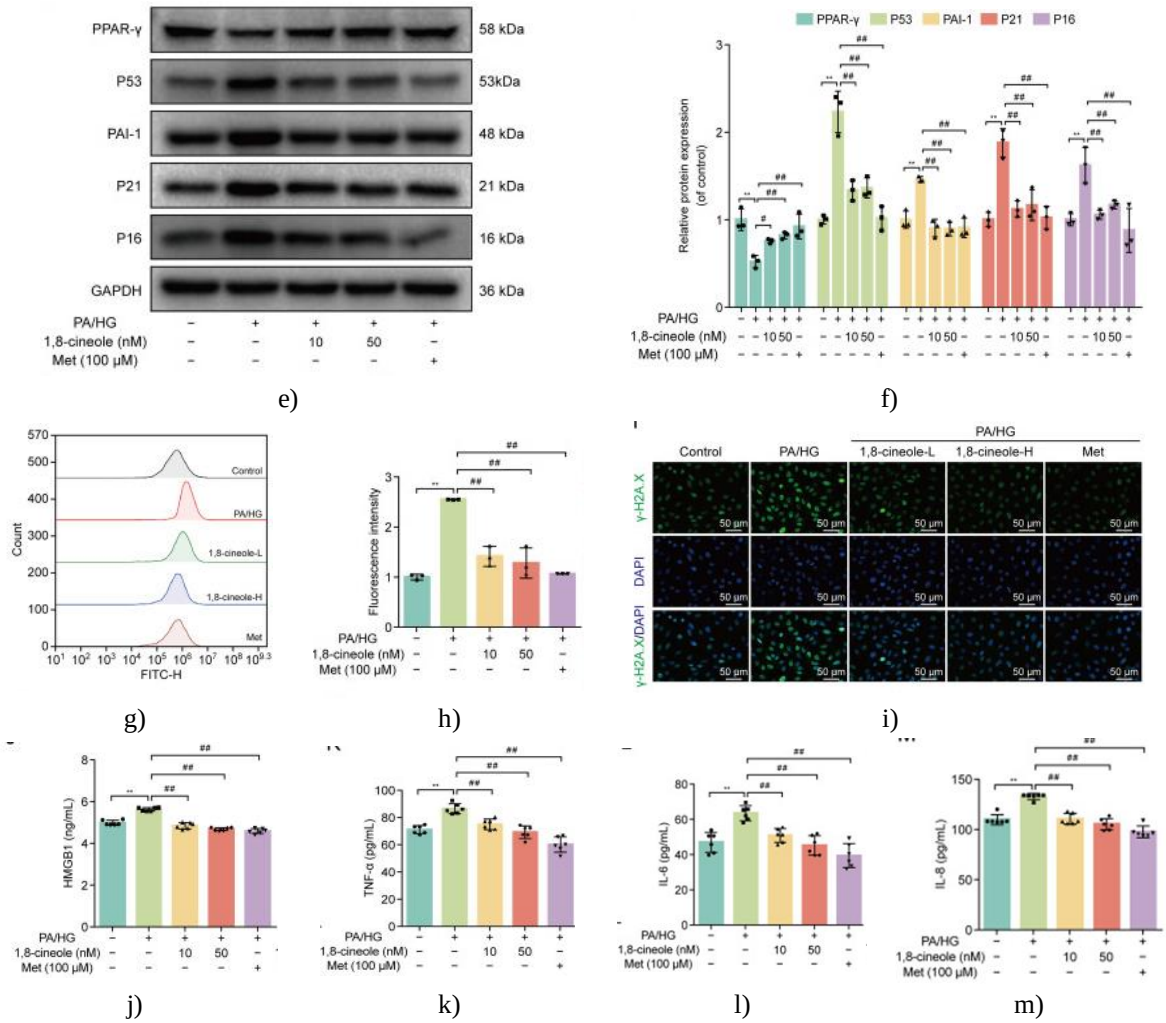

Figure 6. 1, 8-Cineole counters senescence induced by high palmitic acid and high glucose (PA/HG) in human aortic endothelial cells (HAECs). (a) Identification of senescent cells through senescence-associated β-galactosidase (SA-β-gal) staining. (b) Percentage of SA-β-gal-positive cells (n = 3). (c) 1, 8-Cineole rescued PA/HG-caused accumulation of cells in G0/G1 phase in HAECs. (d) Quantitative breakdown of cell cycle phases (n = 3). (e) Protein expression of peroxisome proliferator-activated receptor-γ (PPAR-γ), p53 (P53), plasminogen activator inhibitor-1 (PAI-1), cyclin-dependent kinase inhibitor 1A (P21), and cyclin-dependent kinase inhibitor 2A (P16) assessed by Western blotting in HAECs. (f) Quantified band intensities for PPAR-γ, P53, PAI-1, P21, and P16 from Western blots (n = 3). (g) 1, 8-Cineole curtailed excessive reactive oxygen species (ROS) production triggered by PA/HG in HAECs. (h) Measured ROS intensity (n = 3). (i) γ-H2A.X foci visualised by immunofluorescence in HAECs (n = 3). (j–m) Secreted levels of high mobility group box 1 (HMGB1) (J), tumor necrosis factor-α (TNF-α) (k), interleukin-6 (IL-6) (l), and interleukin-8 (IL-8) (m) in HAEC culture media (n = 3). Results are mean ± standard deviation (SD). ∗∗P < 0.01 vs. the control, #P < 0.05 and ##P < 0.01 vs. PA/HG. 1, 8-cineole-L: low-dose 1, 8-cineole; 1, 8-cineole-H: high-dose 1, 8-cineole; Met: metformin; GAPDH: glyceraldehyde 3-phosphate dehydrogenase; DAPI: 4′, 6-diamidino-2-phenylindole.

Excessive oxidative stress drives multiple aspects of vascular aging pathology. Intense oxidant exposure harms cellular macromolecules—proteins, fats, and nucleic acids—eventually impairing vessel function and promoting premature aging [24]. In HAECs, PA/HG markedly amplified ROS output, a surge notably blunted by 1, 8-cineole **(Figures 6g and 6h)**. Correspondingly, 1, 8-cineole sharply decreased γ-H2A.X signals, reflecting lessened DNA breakage tied to senescence **(Figure 6i)**. PA/HG also prompted heightened release of SASP components HMGB1, TNF-α, IL-6, and IL-8 into the medium, elevations that 1, 8-cineole significantly tempered **(Figures 6j–6m)**. Overall, 1, 8-cineole combats PA/HG-elicited endothelial senescence by damping ROS overload, genomic injury, and inflammatory secretome production.

1, 8-Cineole suppresses HAEC senescence via PPAR-γ pathway engagement

Pharmacological tools—the activator rosiglitazone and blocker GW9662—were deployed to test whether 1, 8-cineole acts through PPAR-γ. Adding GW9662 wiped out 1, 8-cineole's protective actions, restoring high SA-β-gal activity, persistent G0/G1 blockade, and elevated P53, PAI-1, P21, and P16 abundance **(Figures 7a–7f)**. Co-administration of rosiglitazone with high-dose 1, 8-cineole produced no further gains in cycle progression, marker suppression, or SA-β-gal reduction beyond 1, 8-cineole alone, implying shared downstream signalling with this established PPAR-γ ligand **(Figures 7g–7l)**.

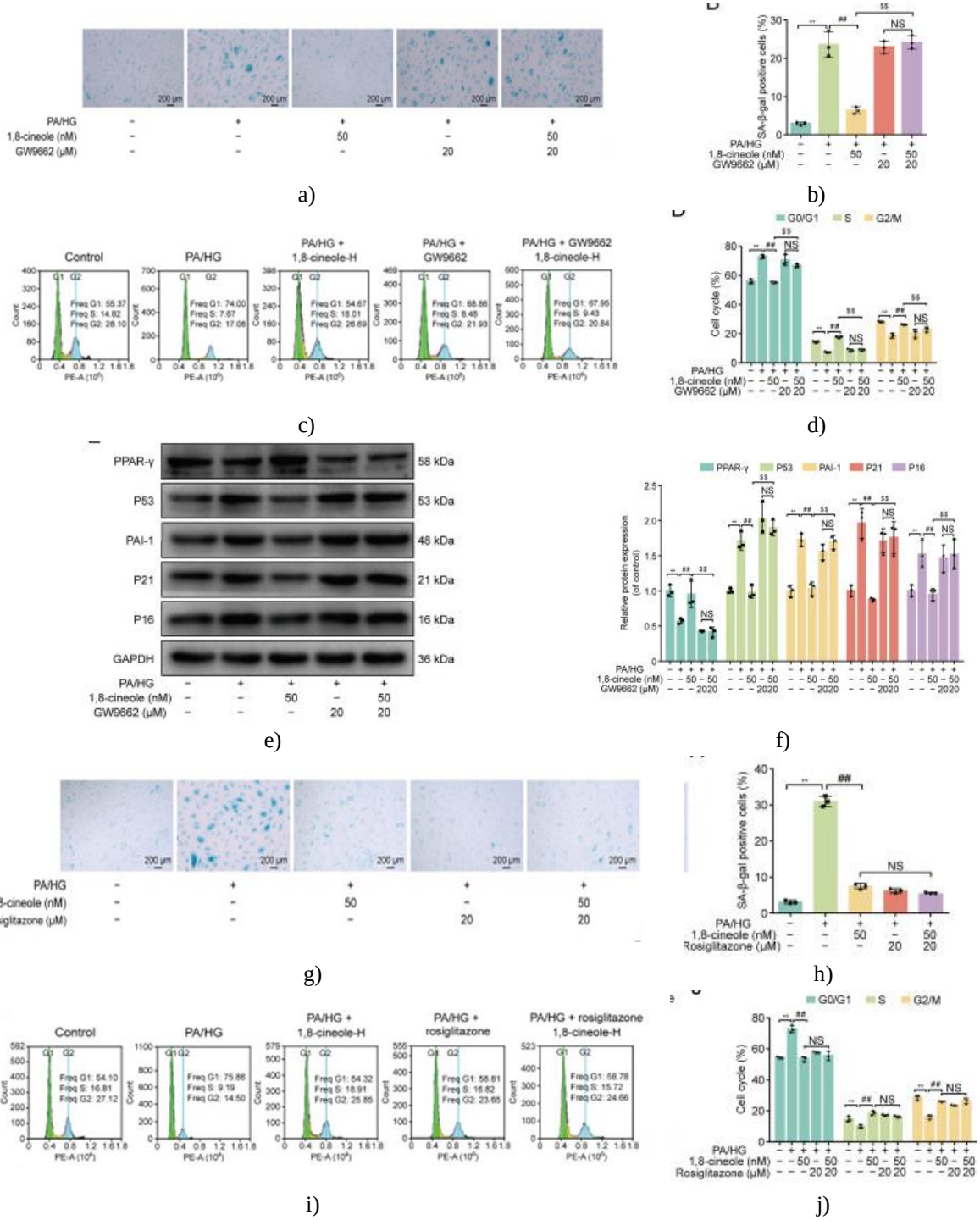

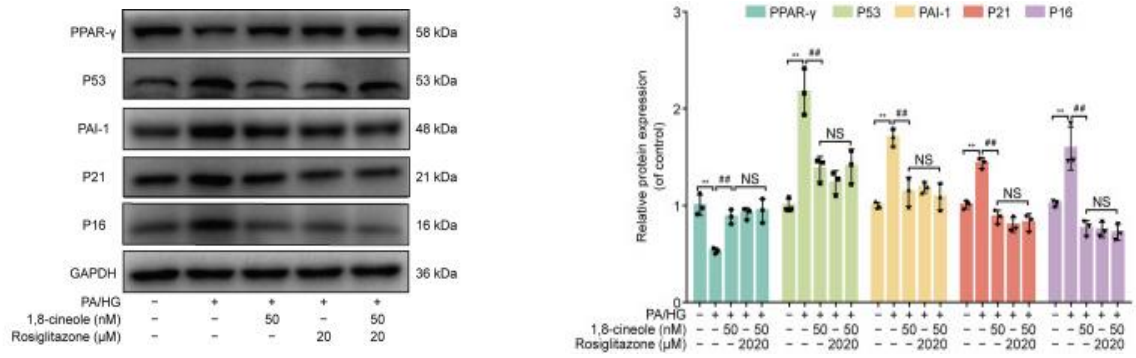

k) l)

Figure 7. 1, 8-Cineole mitigates high palmitic acid/high glucose (PA/HG)-provoked senescence in human aortic endothelial cells (HAECs) by engaging peroxisome proliferator-activated receptor-γ (PPAR-γ) signalling. (a) Example SA-β-gal staining from groups receiving GW9662. (b) Count of SA-β-gal-positive cells (n = 3). (c) Cell cycle distributions under GW9662 influence. (d) Phase-specific cell cycle quantification (n = 3). (e) Western blot evaluation of PPAR-γ, p53 (P53), plasminogen activator inhibitor-1 (PAI-1), cyclin-dependent kinase inhibitor 1A (P21), and cyclin-dependent kinase inhibitor 2A (P16) in GW9662-exposed HAECs. (f) Band density analysis for PPAR-γ, P53, PAI-1, P21, and P16 (n = 3). (g) Example SA-β-gal staining from rosiglitazone-exposed groups. (h) Count of SA-β-gal-positive cells (n = 3). (i) Cell cycle distributions under rosiglitazone influence. (j) Phase-specific cell cycle quantification (n = 3). (k) Western blot evaluation of PPAR-γ, P53, PAI-1, P21, and P16 in rosiglitazone-exposed HAECs. (l) Band density analysis for PPAR-γ, P53, PAI-1, P21, and P16 (n = 3). Results are mean ± standard deviation (SD). ∗∗P < 0.01 vs. the control, ##P < 0.01 vs. PA/HG, $$P < 0.01 vs. PA/HG + 1, 8-cineole, NS: no significance. 1, 8-cineole-H: high-dose 1, 8-cineole; GAPDH: glyceraldehyde 3-phosphate dehydrogenase.

Genetic loss-of-function studies followed, using PPAR-γ-targeted siRNA in HAECs. Effective silencing was verified by substantial drops in both mRNA and protein **(Figures 8a–8c)**. Depleting PPAR-γ abolished 1, 8-cineole's capacity to lower SA-β-gal staining and restore cycle dynamics **(Figures 8d–8f)**. Moreover, knockdown amplified P53, PAI-1, P21, and P16 accumulation **(Figures 8g and 8h)**. These convergent pharmacological and genetic data confirm that 1, 8-cineole safeguards vascular endothelial cells from PA/HG-driven senescence predominantly by stimulating PPAR-γ signalling.

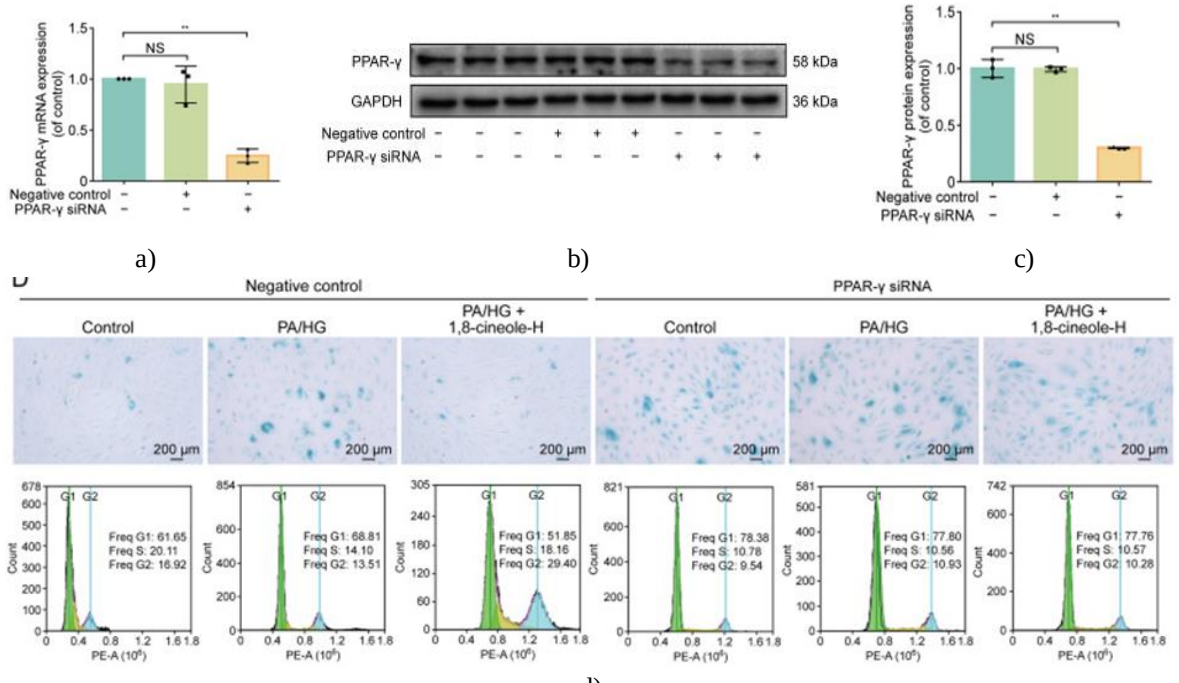

a) b) c)

d)

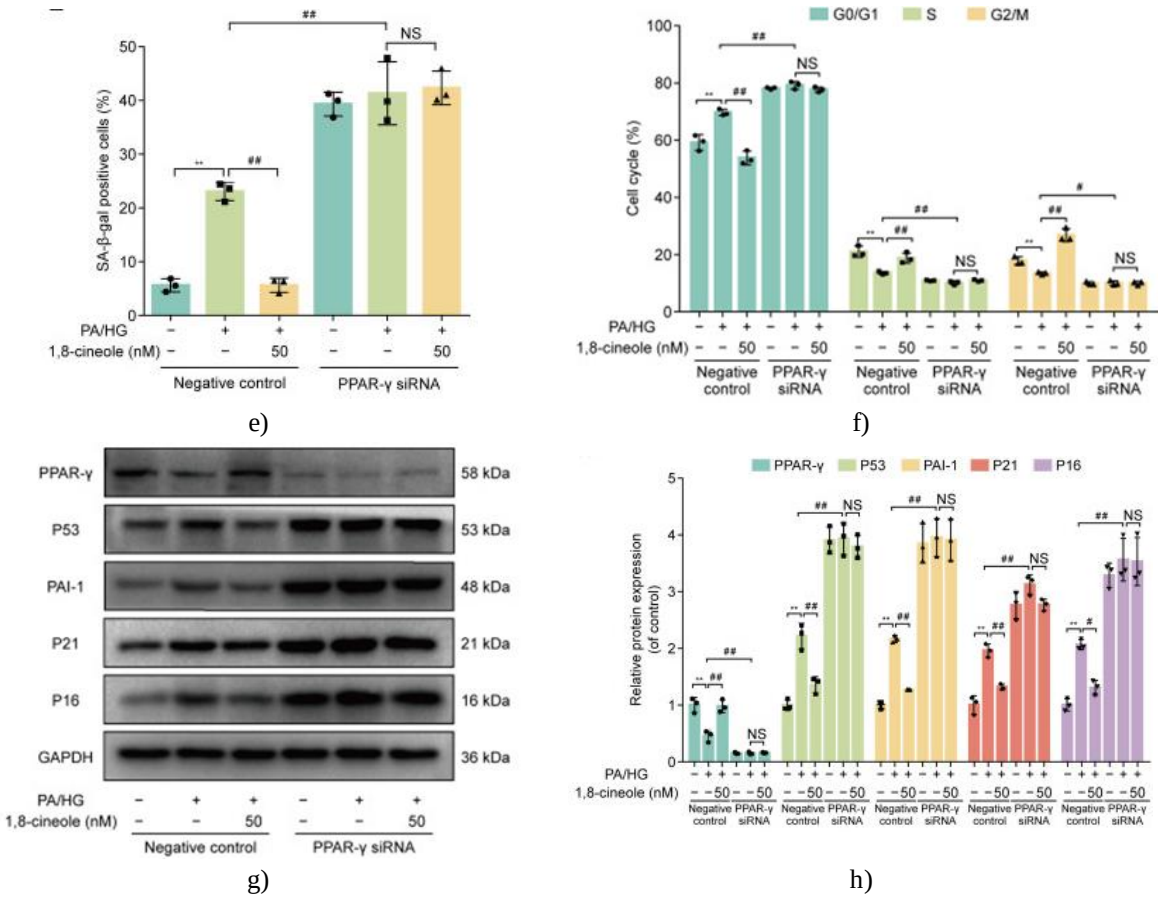

Figure 8. Silencing PPAR-γ removes the senescence-protective role of 1, 8-cineole in human aortic endothelial cells (HAECs). (a) Relative PPAR-γ mRNA in HAECs after transfection with negative control or PPAR-γ-targeted siRNA, quantified by RT-qPCR (n = 3). (b) PPAR-γ protein in negative control- versus PPAR-γ siRNA-transfected HAECs, shown by Western blot. (c) Densitometry for PPAR-γ protein bands (n = 3). (d) Example images of SA-β-gal staining and cell cycle analysis in transfected HAECs under PA/HG stress with or without 1, 8-cineole (n = 3). (e) Percentage of SA-β-gal-positive cells across conditions (n = 3). (f) Cell cycle phase percentages (n = 3). (g) Western blot profiling of PPAR-γ, p53 (P53), plasminogen activator inhibitor-1 (PAI-1), cyclin-dependent kinase inhibitor 1A (P21), and cyclin-dependent kinase inhibitor 2A (P16) in transfected HAECs subjected to PA/HG and/or 1, 8-cineole. (h) Quantified band densities for PPAR-γ, P53, PAI-1, P21, and P16 (n = 3). Values are mean ± standard deviation (SD). ∗∗P < 0.01 vs. the control + negative control, #P < 0.05 and ##P < 0.01 vs. PA/HG + negative control, NS: no significance. 1, 8-cineole-H: high-dose 1, 8-cineole; GAPDH: glyceraldehyde 3-phosphate dehydrogenase.

1, 8-Cineole prevents PPAR-γ breakdown through deubiquitination at Lys-466

RT-qPCR data demonstrated that 1, 8-cineole lowered PA/HG-upregulated mRNA for P53, PAI-1, P21, and P16 without altering PPAR-γ transcript levels. PPAR-γ blockade worsened senescence and cancelled 1, 8-cineole protection. Protein lifespan experiments with cycloheximide (CHX) to block synthesis revealed faster PPAR-γ decay under PA/HG, which 1, 8-cineole delayed, evidencing post-translational control **(Figure 9a)**. Major degradation routes involve autophagy–lysosome or ubiquitin–proteasome systems [25]. Testing with chloroquine (CQ) versus MG132 showed only proteasome inhibition by MG132 preserved PPAR-γ, confirming ubiquitin–proteasome involvement **(Figure 9b)**. Pull-down assays proved 1, 8-cineole reduced PA/HG-triggered PPAR-γ polyubiquitination **(Figure 9c)**. Mass spectrometry pinpointed candidate sites K170, K466, and K485 **(Figure 9d)**. Mutating each lysine to arginine in Flag-PPAR-γ constructs expressed in HEK293T cells singled out Lys-466 as the residue where 1, 8-cineole interferes with ubiquitination **(Figure 9e)**. Hence, 1, 8-cineole boosts PPAR-γ levels by removing ubiquitin chains at Lys-466, thereby blocking PA/HG-driven endothelial aging in HAECs.

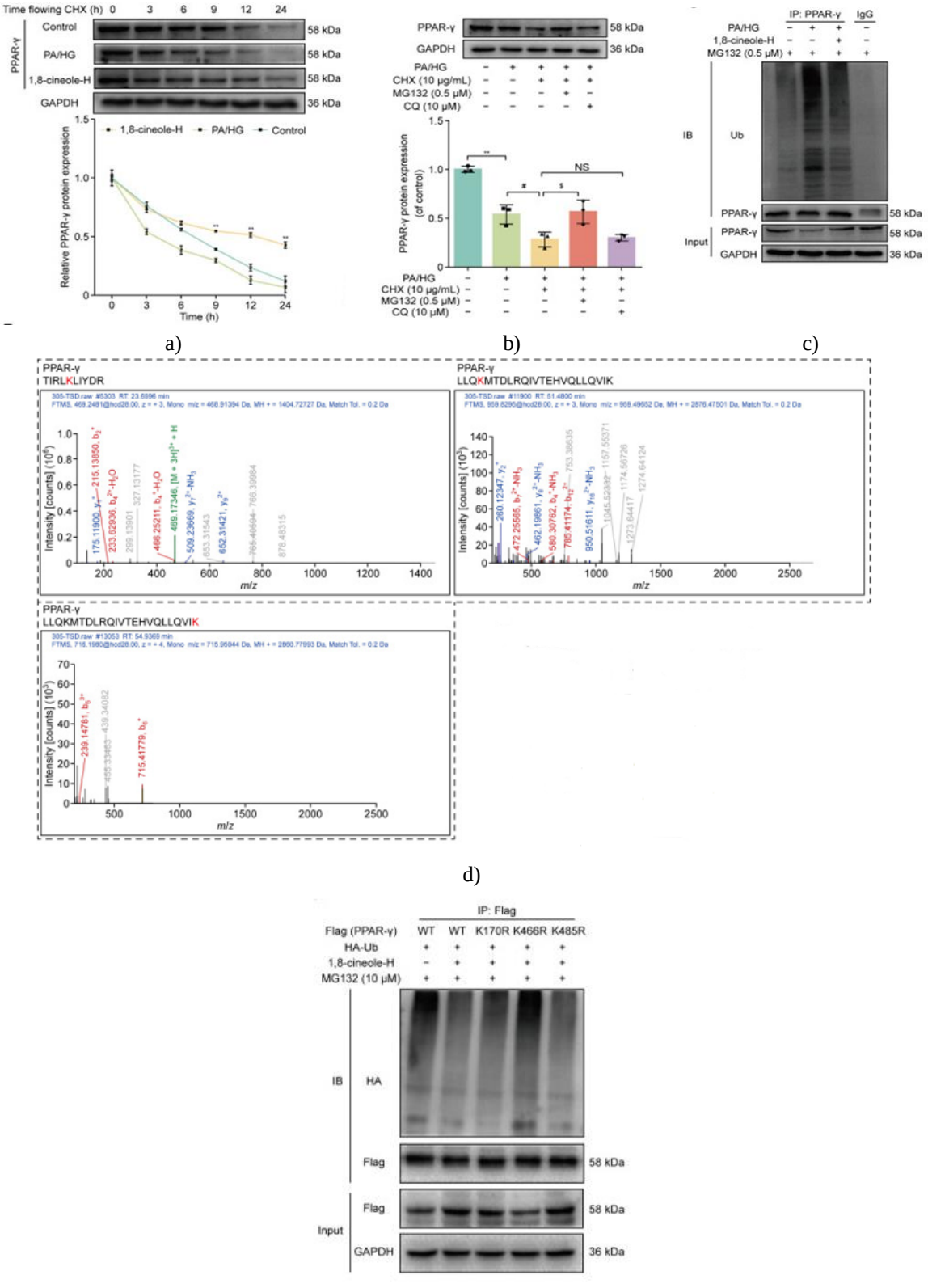

Figure 9. 1, 8-Cineole hinders ubiquitin-mediated loss of peroxisome proliferator-activated receptor-γ (PPAR-γ) at Lys-466. (a) Time-course PPAR-γ protein monitoring in HAECs under PA/HG and/or 1, 8-cineole with cycloheximide (CHX; 10 μg/mL) at 0, 3, 6, 9, 12, or 24 h via Western blot (n = 3). (b) PPAR-γ levels in PA/HG-challenged HAECs with CHX plus chloroquine (CQ) or MG132, detected by Western blot (n = 3). (c) Attenuated PPAR-γ ubiquitination by 1, 8-cineole during PA/HG exposure in HAECs (n = 3). (d) Mass spectrometry-identified PPAR-γ ubiquitination lysines. (e) Western blots from HEK293T cells expressing HA-Ub alongside Flag-PPAR-γ wild-type or K170R, K466R, K485R mutants after Flag pull-

down, detected with HA, Flag, and GAPDH antibodies. Values are mean ± standard deviation (SD). ∗∗P < 0.01 vs. the control, #P < 0.05 vs. PA/HG, $P < 0.05 vs. PA/HG + CHX, NS: no significance. 1, 8-cineole-H: high-dose 1, 8-cineole; Ub: ubiquitin; IgG: immunoglobulin G.

1, 8-Cineole curbs vascular aging in HFD/STZ T2DM mice by engaging PPAR-γ signalling

Aortic PPAR-γ depletion was achieved via tail-vein adenoviral delivery in T2DM mice to test pathway necessity. Successful targeting was evident from aortic GFP expression **(Figure 10a)** and clear PPAR-γ protein decline relative to control + AD-NC **(Figures 10b and 10c)**. Loss of PPAR-γ largely negated 1, 8-cineole's repairs to vessel morphology and excess collagen **(Figure 10d)**. Beneficial shifts in lipid parameters induced by 1, 8-cineole were similarly disrupted (HDL excepted) **(Figures 10e–10h)**. Knockdown also erased 1, 8-cineole's regulation of senescence-associated proteins **(Figures 10i and 10j)**. Collectively, these in vivo results establish that 1, 8-cineole restrains vascular aging in the HFD/STZ T2DM setting mainly through PPAR-γ pathway stimulation.

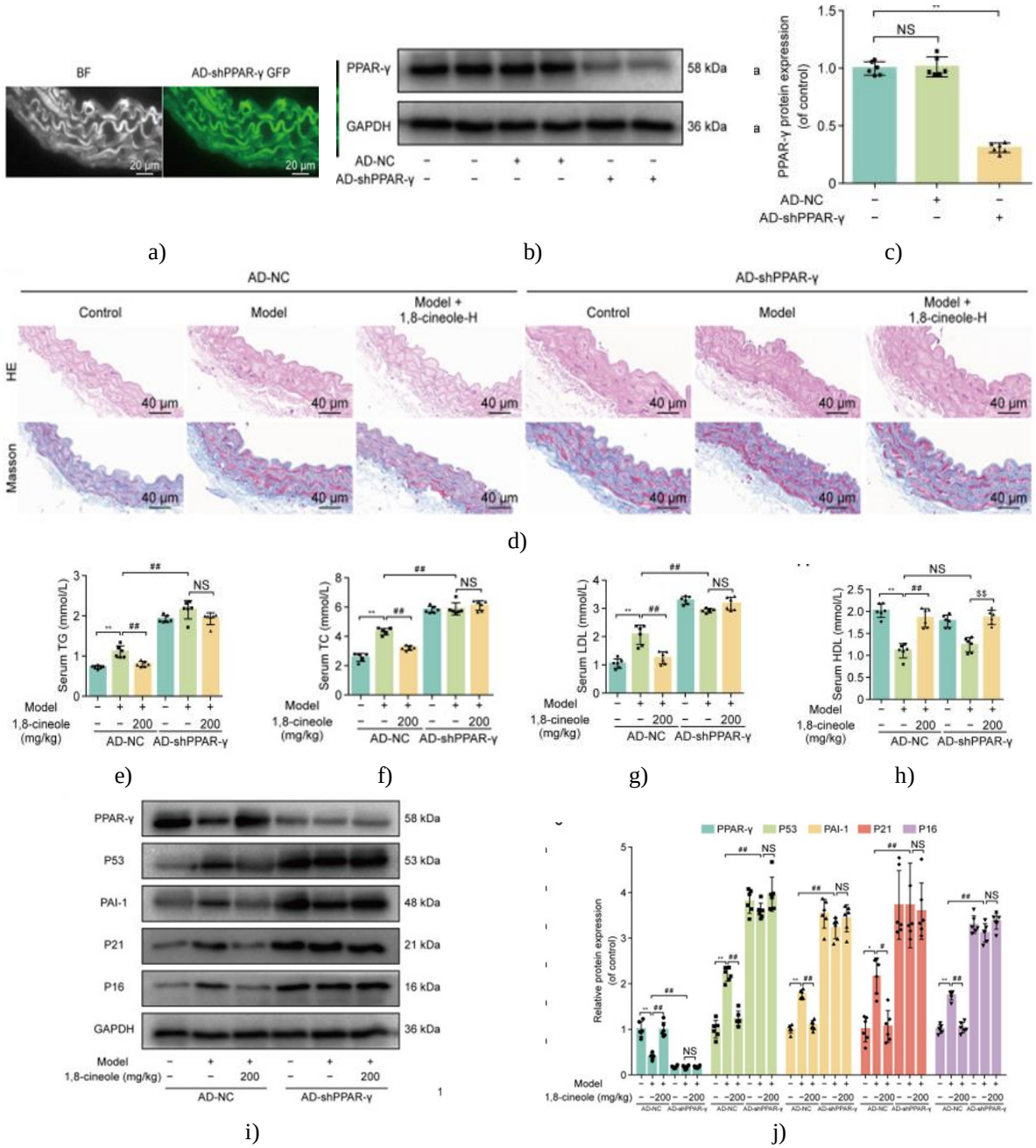

Figure 10. Depletion of peroxisome proliferator-activated receptor-γ (PPAR-γ) eliminates 1, 8-cineole's protection against diabetic vascular aging. (a) Typical green fluorescent protein (GFP) fluorescence in aortas from adenovirus (AD)-injected mice. (b) Western blot detection of PPAR-γ in aortas from AD-transduced

animals. (c) Quantified PPAR-γ protein levels (n = 6). (d) Example haematoxylin and eosin (HE) and Masson trichrome staining of aortic sections post AD delivery (n = 3). (e–h) Circulating triglycerides (TG) (e), total cholesterol (TC) (f), low-density lipoprotein cholesterol (LDL) (g), and high-density lipoprotein cholesterol (HDL) (h) concentrations in AD-injected mice (n = 6). (i) Western blot profiling of PPAR-γ, p53 (P53), plasminogen activator inhibitor-1 (PAI-1), cyclin-dependent kinase inhibitor 1A (P21), and cyclin-dependent kinase inhibitor 2A (P16) in thoracic aortic samples after AD administration. (j) Densitometric analysis of PPAR-γ, P53, PAI-1, P21, and P16 bands (n = 6). Values are mean ± standard deviation (SD). ∗P < 0.05 and ∗∗P < 0.01 vs. the control + AD-NC, #P < 0.05 and ##P < 0.01 vs. model + AD-NC, $$P < 0.01 vs. model + AD-shPPAR-γ, NS: no significance. 1, 8-cineole-H: high-dose 1, 8-cineole; AD-NC: adenovirus-negative control; AD-shPPAR-γ: PPAR-γ short hairpin RNA adenovirus; GAPDH: glyceraldehyde 3-phosphate dehydrogenase.

Diabetes mellitus (DM) is a life-threatening chronic metabolic disorder, with vascular complications representing the leading cause of mortality [26]. Endothelial senescence in vessels is a pivotal contributor to these DM-related issues, yet the precise molecular drivers remain incompletely defined [27]. Discovering agents capable of suppressing vascular endothelial aging is therefore essential to reduce DM-associated vascular morbidity and death.

Traditional Chinese medicine (TCM), with thousands of years of clinical use, is extensively applied in China for health promotion and holds considerable potential for managing cardiovascular conditions. Numerous reports highlight potent anti-diabetic actions of TCM-derived compounds [28]. Notably, 1, 8-cineole exhibits diverse bioactivities including anti-inflammatory, antioxidative, antimicrobial, bronchodilator, analgesic, and pro-apoptotic properties [29]. Earlier work has linked 1, 8-cineole to diabetes prevention, showing attenuation of endothelial injury, restoration of endothelial and mitochondrial function, and favourable shifts in inflammation and lipid handling [30, 31]. Still, detailed insights into its influence on diabetic vascular endothelial aging and the precise pathways involved have been lacking.

In this work, we delineated the therapeutic actions and primary molecular target of 1, 8-cineole in combating DM-linked vascular aging. Reliable models of endothelial senescence were generated in T2DM mice and HAECs to evaluate 1, 8-cineole efficacy. Our data robustly showed that 1, 8-cineole counters DM-driven vascular endothelial aging via PPAR-γ pathway stimulation. This engagement decreased senescent cell counts, eased cycle blockade, dampened aging-related inflammation, normalised lipids, lowered senescence marker abundance, and slowed diabetic endothelial aging progression. Additionally, 1, 8-cineole diminished ROS buildup and γ-H2A.X signals—established hallmarks of oxidative stress and genomic injury in aging. These collective outcomes position 1, 8-cineole as a promising candidate for managing diabetic vascular endothelial aging.

We integrated GEO clinical datasets comparing diabetic and non-diabetic individuals with entries from OMIM, GeneCards, and DisGeNET to pinpoint DM- and aging-associated genes. Candidate prioritisation employed molecular docking and MD simulation instead of standard network pharmacology approaches. PPAR-γ emerged as the leading prospect for DM-associated aging. PPAR-γ stimulation is vital for lipid handling, insulin sensitivity, and vascular homeostasis [32, 33]. Activation also curbs senescent cell accumulation, relieves cycle arrest, and downregulates aging proteins, thereby retarding endothelial senescence [19]. Aligning with this, we observed marked PPAR-γ decline in PA/HG-challenged HAECs and T2DM mouse aortas, reversible upon 1, 8-cineole exposure.

CETSA and DARTS, established ligand-induced stability assays [34, 35], both indicated high-affinity interaction, with 1, 8-cineole enhancing PPAR-γ resistance to heat and proteolysis. SPR quantified binding at 23.8 μM affinity constant, reinforcing direct engagement. Thus, PPAR-γ stands confirmed as the core target of 1, 8-cineole and a central player in diabetic endothelial aging. Critically, PPAR-γ antagonism by GW9662 or genetic silencing reversed 1, 8-cineole's anti-senescence benefits—including senescent cell reduction, cycle rescue, and marker suppression. In contrast, the agonist rosiglitazone offered no additive activation beyond 1, 8-cineole, implying mechanistic overlap. Overall, 1, 8-cineole exerts its vascular endothelial anti-aging effects in diabetes predominantly through PPAR-γ pathway engagement.

Protein levels are governed by the equilibrium between synthesis and breakdown. Notably, our data revealed that 1, 8-cineole substantially elevated PPAR-γ protein abundance without affecting PPAR-γ mRNA, implying that its influence on PPAR-γ occurs post-transcriptionally rather than through transcriptional control. Half-life experiments for PPAR-γ protein supported this interpretation. The ubiquitin–proteasome and autophagy–

lysosome systems are primary routes for protein turnover [36, 37]. Treatment with MG132 (proteasome inhibitor) versus CQ (autophagy inhibitor) established that PPAR-γ clearance proceeds via the ubiquitin–proteasome route. This aligns with prior observations [10]. Dysregulated ubiquitination contributes to multiple aging processes, including senescence [38]. Crucially, we found heightened PPAR-γ ubiquitination at Lys-466 correlated with reduced protein levels in PA/HG-stressed senescent cells.

Earlier reports indicated that 1, 8-cineole mitigates dyslipidemia and vascular lesions in T2DM mice [16, 30, 31]. The current work extends this by showing that 1, 8-cineole not only corrects lipid imbalances and aortic structural defects in T2DM models but also suppresses inflammatory cytokines (TNF-α, HMGB1, IL-6, and IL-8), senescence markers (P53, PAI-1, P21, and P16), and the DNA damage indicator γ-H2A.X. These actions collectively alleviate lipid disorders, vascular pathology, aging-linked inflammation, and genomic injury, ultimately postponing endothelial senescence in diabetic mice. To substantiate PPAR-γ involvement, we depleted aortic PPAR-γ in T2DM mice using tail-vein adenoviral delivery. Outcomes mirrored in vitro silencing, with loss of PPAR-γ abolishing 1, 8-cineole's anti-senescence benefits. In aggregate, our evidence robustly supports that 1, 8-cineole counters diabetic vascular endothelial aging by engaging PPAR-γ and blocking its ubiquitination-mediated degradation specifically at Lys-466.

Despite providing strong support for 1, 8-cineole's efficacy against diabetic vascular endothelial aging, this study has limitations. Firstly, effects in female mice were not examined. Additionally, aortic PPAR-γ knockdown relied on tail-vein adenoviral injection; although validated by Western blotting and fluorescence imaging, prior studies note that adenoviruses can drive ectopic gene expression or silencing in vessels [39-41]. Conditional PPAR-γ knockout models could offer greater specificity. Lastly, while ubiquitination sites on PPAR-γ were mapped, the detailed regulatory machinery warrants deeper exploration, including functional consequences of the identified mutation site.

Conclusion

For the first time, this investigation clarifies that 1, 8-cineole safeguards against diabetic vascular endothelial aging by promoting PPAR-γ deubiquitination at Lys-466 and thereby enhancing its stability. As a promising therapeutic agent, 1, 8-cineole may lay theoretical and experimental groundwork for advancing traditional Chinese medicine applications in managing DM-associated vascular complications.

Acknowledgments: None

Conflict of Interest: None

Financial Support: None

Ethics Statement: None

References

1. Wu Y, Ding Y, Tanaka Y, Zhang W. Risk factors contributing to type 2 diabetes and recent advances in the treatment and prevention. Int J Med Sci. 2014;11:1185–200.
2. Tai G, Yu Q, Li J, Zhang L, Wang H, Liu Y, et al. NLRP3 inflammasome links vascular senescence to diabetic vascular lesions. Pharmacol Res. 2022;178:106143.
3. Li J, Yang Z, Song H, Chen X, Zhang Y, Liu L, et al. The role of mitofusin 2 in regulating endothelial cell senescence. iScience. 2024;27:110809.
4. Ou H, Schumacher B. DNA damage responses and p53 in the aging process. Blood. 2018;131:488–95.
5. Patel J, Baptiste BA, Kim E, Hussain M, Croteau DL, Bohr VA. DNA damage and mitochondria in cancer and aging. Carcinogenesis. 2020;41:1625–34.
6. Villarroel-Vicente C, Gutierrez-Palomo S, Ferri J, Rodríguez-García C, Sánchez-Moreno C, León R, et al. Natural products and analogs as preventive agents for metabolic syndrome via PPARs. Eur J Med Chem. 2021;221:113535.
7. Wan R, Srikaram P, Xie S, Chen H, Zhao Y, Li J, et al. PPARγ attenuates cellular senescence of alveolar macrophages in asthma-COPD overlap. Respir Res. 2024;25:174.

8. Heng Y, Wei W, Cheng L, Liu X, Zhang J, Wang Y, et al. FGF21 alleviates VSMC senescence in diabetic mice. Acta Biochim Biophys Sin (Shanghai). 2024;56:892–904.
9. Jiang Z, Hao F, Zhu F, Liu Y, Chen X, Wang Q, et al. RSL1D1 modulates cell senescence via regulation of PPARγ mRNA stability. Life Sci. 2022;307:120848.
10. Qiu J, Shu C, Li X, Zhang Y, Wang Z, Liu H, et al. PAQR3 depletion accelerates diabetic wound healing via angiogenesis. Lab Invest. 2022;102:1121–31.
11. Kim SG, Sung JY, Kang YJ, Lee YH, Kim DH, Lee SH, et al. PPARγ activation by fisetin mitigates vascular smooth muscle cell senescence via the mTORC2-FoxO3a-autophagy signaling pathway. Biochem Pharmacol. 2023;218:115892.
12. Xu L, Ma X, Verma N, Wang D, Gavrilova O, Proia RL, et al. PPARγ agonists delay age-associated metabolic disease and extend longevity. Aging Cell. 2020;19:e13267.
13. Cai Z, Peng J, Chen Y, Tao L, Zhang Y, Fu X, et al. 1,8-Cineole: A review of source, biological activities, and application. J Asian Nat Prod Res. 2021;23:938–54.
14. Linghu K, Lin D, Yang H, Wu G, Fu L, Zhang X, et al. Ameliorating effects of 1,8-cineole on LPS-induced endothelial cell injury via NF-κB suppression. Eur J Pharmacol. 2016;789:195–201.
15. Linghu K, Wu G, Fu L, Yang H, Zhang X, Liu Y, et al. 1,8-Cineole ameliorates vascular endothelium dysfunction via PPARγ-dependent NF-κB regulation. Front Pharmacol. 2019;10:178.
16. Liu Z, Gan S, Fu L, Zhang X, Wu G, Linghu K, et al. 1,8-Cineole ameliorates diabetic retinopathy via PPARγ/TXNIP pathways. Biomed Pharmacother. 2023;164:114978.
17. Venkataraman B, Almarzooqi S, Raj V, Nair A, Nair S, Pillai R, et al. Molecular docking identifies 1,8-cineole as a novel PPARγ agonist. Int J Mol Sci. 2023;24:6160.
18. Valdés-Tresanco MS, Valdés-Tresanco ME, Valiente PA, Moreno E. gmx_MMPBSA: A tool for free energy calculations with GROMACS. J Chem Theory Comput. 2021;17:6281–91.
19. Liao J, Fu L, Tai S, Zhang X, Wu G, Linghu K, et al. Essential oil ameliorates endothelial cell senescence in diabetes via PPARγ signaling. J Ethnopharmacol. 2024;321:117550.
20. Singh R, Gholipourmalekabadi M, Shafikhani SH. Animal models for type 1 and type 2 diabetes: Advantages and limitations. Front Endocrinol (Lausanne). 2024;15:1359685.
21. Burton DGA, Faragher RGA. Obesity and type-2 diabetes as inducers of premature cellular senescence and ageing. Biogerontology. 2018;19:447–59.
22. Abdullah KM, Alam MM, Iqbal Z, Siddiqui AA, Ansari SH, Najmi AK, et al. Therapeutic effect of vitamin B3 on hyperglycemia, oxidative stress and DNA damage in alloxan-induced diabetic rat model. Biomed Pharmacother. 2018;105:1223–31.
23. Hemmings KE, Riches-Suman K, Bailey MA, et al. Role of microRNA-145 in DNA damage signalling and senescence in vascular smooth muscle cells of type 2 diabetic patients. Cells. 2021;10:919.
24. Maldonado E, Morales-Pison S, Urbina F, et al. Aging hallmarks and the role of oxidative stress. Antioxidants (Basel). 2023;12:651.
25. Ihara Y, Morishima-Kawashima M, Nixon R. The ubiquitin-proteasome system and the autophagic-lysosomal system in Alzheimer disease. Cold Spring Harb Perspect Med. 2012;2:a006361.
26. Xiang H, Song R, Ouyang J, Zhang Y, Li X, Chen Y, et al. Organelle dynamics of endothelial mitochondria in diabetic angiopathy. Eur J Pharmacol. 2021;895:173865.
27. Zhu S, Wang M, He Y, Liu X, Zhang J, Li Z, et al. Capsaicin ameliorates endothelial senescence via TRPV1/SIRT1 pathway. Phytomedicine. 2022;100:154081.
28. Tao M, Zheng D, Liang X, Chen Y, Wang H, Li X, et al. Tripterygium glycoside suppresses EMT in diabetic kidney disease via autophagy regulation. Mol Med Rep. 2021;24:592.
29. Hoch CC, Petry J, Griesbaum L, et al. 1,8-Cineole: A versatile phytochemical with therapeutic applications. Biomed Pharmacother. 2023;167:115467.
30. Yang H, Chen Y, Linghu K, Wu G, Fu L, Zhang X, et al. 1,8-Cineole alleviates redox imbalance via Sirt1 in diabetes. Phytomedicine. 2024;135:156099.
31. Zhang J, Li X, Cui W, Wang Y, Chen Y, Liu Z, et al. 1,8-Cineole ameliorates diabetic angiopathy via inhibition of NLRP3 inflammasome-mediated pyroptosis. Biomed Pharmacother. 2024;177:117085.
32. Wagner N, Wagner KD. Pharmacological utility of PPAR modulation for angiogenesis in cardiovascular disease. Int J Mol Sci. 2023;24:2345.

33. De Silva TM, Li Y, Kinzenbaw DA, et al. Endothelial PPARγ is essential for preventing endothelial dysfunction with aging. Hypertension. 2018;72:227–34.
34. Cai X, Jiang X, Zhao M, Zhang Y, Li Y, Wang X, et al. Identification of honokiol target protein and mechanism in anti-inflammatory action. Phytomedicine. 2023;109:154617.
35. Chen F, Li C, Cao H, Zhang Y, Wang X, Liu Y, et al. Identification of adenylate kinase 5 as ginsenoside target protein. J Agric Food Chem. 2022;70:2741–51.
36. Heo AJ, Ji CH, Kwon YT. The Cys/N-degron pathway in ubiquitin-proteasome system and autophagy. Trends Cell Biol. 2023;33:247–59.
37. Li Y, Li S, Wu H, Zhang Y, Wang X, Chen Y, et al. UPS and autophagy in response to cellular stress. Cells. 2022;11:851.
38. Xiang H, Yuan Q, Zeng J, Chen Y, Liu X, Zhang Y, et al. MDM2 accelerates renal senescence via HDAC1 degradation. Acta Pharmacol Sin. 2024;45:2328–38.
39. Wang S, Yang S, Chen Y, Li X, Zhang J, Liu Y, et al. Ginsenoside Rb2 alleviates atherosclerosis via macrophage polarization inhibition. Front Pharmacol. 2022;12:764130.
40. Okuyama M, Uchida HA, Umebayashi R, et al. Vasohibin-2 exacerbates angiotensin II-induced aortic aneurysm. Arterioscler Thromb Vasc Biol. 2017;37:A640.
41. Sun Y, Chen C, Xue R, Wang Y, Liu X, Zhang J, et al. Maf1 ameliorates cardiac hypertrophy by inhibiting RNA polymerase III through ERK1/2. Theranostics. 2019;9:7268–81.